

DESIGN OF A PINTLE INJECTOR

A THESIS SUBMITTED TO  
THE GRADUATE SCHOOL OF NATURAL AND APPLIED SCIENCES  
OF  
MIDDLE EAST TECHNICAL UNIVERSITY

BY

BERKSU ERKAL

IN PARTIAL FULFILLMENT OF THE REQUIREMENTS  
FOR  
THE DEGREE OF MASTER OF SCIENCE  
IN  
MECHANICAL ENGINEERING

SEPTEMBER 2019



Approval of the thesis:

**DESIGN OF A PINTLE INJECTOR**

submitted by **BERKSU ERKAL** in partial fulfillment of the requirements for the degree of **Master of Science in Mechanical Engineering Department, Middle East Technical University** by,

Prof. Dr. Halil Kalıpçılar  
Dean, Graduate School of **Natural and Applied Sciences**

\_\_\_\_\_

Prof. Dr. Sahir Arıkan  
Head of Department, **Mechanical Engineering**

\_\_\_\_\_

Prof. Dr. Mehmet Haluk Aksel  
Supervisor, **Mechanical Engineering, METU**

\_\_\_\_\_

**Examining Committee Members:**

Assoc. Prof. Dr. Cüneyt Sert  
Mechanical Engineering, METU

\_\_\_\_\_

Prof. Dr. Mehmet Haluk Aksel  
Mechanical Engineering, METU

\_\_\_\_\_

Assoc. Prof. Dr. M. Metin Yavuz  
Mechanical Engineering, METU

\_\_\_\_\_

Assist. Prof. Dr. Özgür Uğraş Baran  
Mechanical Engineering, METU

\_\_\_\_\_

Assist. Prof. Dr. Onur Baş  
Mechanical Engineering, TED University

\_\_\_\_\_

Date: 09.09.2019

**I hereby declare that all information in this document has been obtained and presented in accordance with academic rules and ethical conduct. I also declare that, as required by these rules and conduct, I have fully cited and referenced all material and results that are not original to this work.**

Name, Surname: Berksu Erkal

Signature:

## **ABSTRACT**

### **DESIGN OF A PINTLE INJECTOR**

Erkal, Berksu  
Master of Science, Mechanical Engineering  
Supervisor: Prof. Dr. Mehmet Haluk Aksel

September 2019, 84 pages

Pintle injector design methodology for liquid oxygen/gaseous methane rocket engine is investigated with this study. Cold flow experimental work is conducted with water and air to investigate the characteristics of designed injectors by observing spray formations. 750N at maximum thrust with 3:1 throttle ability is chosen as mission requirement. 3 different reservoir geometries are manufactured and experimental investigation is conducted to ensure uniform and axisymmetric spray cone. After decision of the final reservoir, 6 different injectors are designed which are combination of 3 different pintle angles and 2 different annular gap thickness. Non-dimensional parameters from literature are used to determine water and air mass flow rates of cold flow experiments. Phase Doppler Particle Analyzer (PDPA) is utilized to obtain droplet Sauter mean diameters (SMD) and velocity profile in axial and radial direction within the spray. These experiments are carried out for 3 different throttle level for all injectors designed. Spray half cone angles are measured by high speed camera and high contrast images are obtained for post processing observations. At studied flow rates recirculation zone is obtained only for 20° instead of 30° and 40° pintle angles and Sauter Mean Diameter (SMD) increase is experienced at the end of these recirculation zones. Moreover, wider spray half angles up to 58° are obtained with the pintle angle of 20°. SMD values are in the range of 20-50 µm for all injector types at

recirculation zones and injectors with 20° pintle angle have the lowest SMD values compared with the other injectors.

Keywords: Pintle Injectors, Throttling, Phase Doppler Particle Analyzer

## ÖZ

### İĞNE UÇLU PÜSKÜRTEÇ TASARIMI

Erkal, Berksu  
Yüksek Lisans, Makina Mühendisliği  
Tez Danışmanı: Prof. Dr. Mehmet Haluk Aksel

Eylül 2019, 84 sayfa

Bu çalışma ile, sıvı oksijen/gaz metan roket motorları için tasarım yöntemi verilmiştir. Sprey karakteristiklerini incelemek için, su ve hava ile soğuk akış testleri gerçekleştirilmiştir. En yüksek itkisi 750N olan ve itkisinin üçte birine indirme kabiliyetine sahip püskürteç tasarımı esas alınarak tasarım süreci başlatılmıştır. Nizami ve eksenel spray elde etmek üzere 3 farklı hazne geometrisi deneysel olarak incelenmiştir. Hazne geometrisi belirlendikten sonra 3 oksitleyici ve 2 yakıt geometrisinin kombinasyonu olacak şekilde 6 farklı püskürteç tasarlanmıştır. Literatürdeki boyutsuz parametreler kullanılarak soğuk akış deneylerinin su ve hava debileri belirlenmiştir. Faz Doppler parçacık analizcisi kullanılarak parçacıkların Sauter ortalama çapları ve hız profilleri elde edilmiştir. 3 farklı itki seviyesinde bu deneyler her püskürteç için gerçekleştirilmiştir. Bunlara ek olarak, hızlı kamera ile spray açıları ölçülmüştür ve test sonrası incelemeler için kontrastı yüksek görseller elde edilmiştir. Çalışılan debilerde sadece 20° açılı iğnelerde döngüsel alanlar oluşmuş, 30° ve 40° iğne açılarında döngüsel alanlar oluşmamıştır. Bu alanların bitişlerinde ise Sauter ortalama çaplarında bir artış gözlemlenmiştir. Ayrıca, 20° açılı iğne uçlarında, 58° püskürteç yarım açısına ulaşılmıştır. Döngüsel alanlarda Sauter ortalama çaplarının 20-50 µm arasında çeşitlendiği gözlemlenmiştir. Bunlara ek

olarak Sauter ortalama aplarının 20° ięne ucunda grece daha dşk olduęu gzlemlenmiřtir.

Anahtar Kelimeler: İęne Ulu Pskrte, İtki Daraltma, Faz Doppler paracık analizcisi

To my family...

## ACKNOWLEDGEMENTS

Firstly, I would like to express my deepest appreciation to my supervisor Prof. Dr. M. Haluk Aksel for his understanding, guidance and vital support throughout the study.

I would like to thank my thesis committee members,

Moreover, I feel lucky that I had a chance to meet with my fellows Onur Baran and Tolga Tokgöz who helped me every time during my study. I also would like to Dr. Bülent Sümer, Chief of Propulsion Systems Division, for his technical support on this work.

I am also glad to have technical support from Caner Ekin Kiper, Halil Arslan and Çetin Ozan Alanyalıođlu, Levent Çaçatay Öz during my study, I would like to thank these helpful people.

In addition to these people, I would like to thank to Dr. Bilsay Sümer for his lab instrument support.

This research has been supported by TÜBİTAK SAGE; thus, I would like to thank to my institute.

Finally, I would like to thank to my family and my love Meltem Tuna for their understanding and support.

## TABLE OF CONTENTS

ABSTRACT .....	v
ÖZ .....	vii
ACKNOWLEDGEMENTS .....	x
TABLE OF CONTENTS .....	xi
LIST OF TABLES .....	xiii
LIST OF FIGURES .....	xiv
LIST OF ABBREVIATIONS .....	xvii
LIST OF SYMBOLS .....	xviii
CHAPTERS	
1. INTRODUCTION .....	1
1.1. Motivation .....	1
1.1.1. Literature Review .....	2
2. Design Procedure .....	21
2.1. Introduction .....	21
2.2. Design of Outlet Region .....	22
2.3. Design of the Inner Geometry .....	26
2.3.1. Alternative Design 1 .....	27
2.3.2. Alternative Design II .....	29
2.3.3. Moveable Mechanism .....	30
3. Experimental Setup And Results .....	33
3.1. Introduction .....	33
3.2. Experimental Equipment .....	33

3.2.1. Droplet Generator.....	33
3.2.2. Phase Doppler Analysis System.....	34
3.2.3. Photodiode Power Sensor.....	36
3.2.4. Linear Actuator.....	36
3.2.5. High Speed Camera.....	37
3.2.6. Traverse System .....	37
3.2.7. Pintle Injector .....	37
3.3. Experimental Methodology.....	38
3.3.1. Shadowgraphy with High Speed Camera.....	38
3.3.2. Phase Doppler Particle Anemometry .....	39
3.4. Experimental Setup and Tests.....	41
3.4.1. Experimental Setup .....	41
3.4.2. Experimental Matrix.....	42
3.4.2.1. PDPA Experiments' Results.....	48
3.4.2.2. Shadowgraph Experiments Results .....	59
4. Conclusion.....	67
REFERENCES .....	71
A. Velocity and SMD Values of Remaining Experiments.....	73

## LIST OF TABLES

### TABLES

Table 1.1 Comparison Between Typical Liquid Rocket Engines and Pintle Engines (Reproduced from [1]) .....	3
Table 1.2 Pintle Engines Manufactured (Reproduced from [3]).....	5
Table 1.3 Geometric Inputs for the Analysis Performed by Son et al (Reproduced form Ref. [7]).....	9
Table 1.4 Mass Flow Rates and Targeted Chamber Pressures for the Analysis Performed by Son et al. (Reproduced form Ref [7]).....	10
Table 2.1. Enter the Table Caption here .....	22
Table 2.2. Tabulated Vesion of Step 4.....	24
Table 2.3 LOX and GCH <sub>4</sub> Mass Flow Rates and Corresponding Pintle Tracing Distance.....	26
Table 3.1Injector Parameters for Each Type.....	37
Table 3.2 Geometric Parameter Calculation For OF=2 Case for Design Condition and Cold Flow Experiment .....	43
Table 3.3 Geometric Parameter Calculation For 3 different Throttle Levels for Injector Type-1 .....	43
Table 3.4 Geometric Parameter Calculation For 3 different Throttle Levels for Injector Type-4 .....	44
Table 3.5 Experimental Matrix for 6 Injector .....	45
Table 3.6 Droplet Generated Droptlets Measured by PDPA System .....	47
Table 3.7 Experiments Performed Other Than Design Condition Simulation .....	63

## LIST OF FIGURES

### FIGURES

Figure 1.1 Lunar Module Descent Engine Pintle Injector [2] .....	4
Figure 1.2. Base Design Geometry Son et al [4] .....	6
Figure 1.3 Experimental Setup of Son et al [4] .....	6
Figure 1.4 a) Base Geometry of the second work of Son et al [4] b) Pintle opening distance vs transition point [4].....	7
Figure 1.5 Cone Angle Defined by Son et al (on left [6] , on right [5] ).....	8
Figure 1.6 Base Geometry of Numerical work of Sun et al [7].....	9
Figure 1.7 4 Different geometries studied by Son et al [7] .....	9
Figure 1.8 Comparison of Post Center Radius Effect From the Study of Son et al [7] .....	10
Figure 1.9. Weber Number-Total Momentum Ratio Relation for 3 Different Pintle Tip Angles [5] .....	12
Figure 1.10 Spray Angle-Characteristic Number Relation for 3 Different Pintle Tip Angles [5] .....	12
Figure 1.11. Velocity Ratios of Son's Study [5] .....	12
Figure 1.12 Comparison with atmospheric tests [15].....	13
Figure 1.13. Base Geometry of Badard et al [8].....	14
Figure 1.14 Components of Pintle Injector Designed by Badard et al [8] .....	15
Figure 1.15. Uniformity of the Jet Intriduced by Bedard [8].....	15
Figure 1.16. Momentum Equation Applied Control Volumes [9].....	16
Figure 1.17 Comparison of 3 Ways to Determine Cone Angle.....	17
Figure 1.18 Injector Configuration of Reference [9].....	17
Figure 1.19 Fuel-Centered Pintle Injector Hot Fire Test Done by Sakaki (Chamber Pressure, PFI: Fuel injection pressure, POI: Oxidizer injection pressure, TOI: Oxidizer injection temperature) [10] .....	18

Figure 1.20 Technical Drawing and Injector Itself of LCPE [11] .....	18
Figure 2.1 Base Geometry for the Design .....	22
Figure 2.2 First Alternative Design for Inner Geometry.....	28
Figure 2.3. Water Flow at Oxidizer Passage for First Alternative Design .....	29
Figure 2.4. Second Alternative Design (Direct Flow Passage).....	30
Figure 2.5. Second Alternative Design from Another Cross Section .....	30
Figure 2.6 Moveable Mechanism with Linear Actuator .....	31
Figure 2.7 A Cross Section of Movable Mechanism .....	31
Figure 2.8. Cross Section of Moveable Mechanism from Top .....	32
Figure 3.1 Droplet Generator System .....	34
Figure 3.2 PDPA System [15].....	35
Figure 3.3 Linear Actuator .....	36
Figure 3.4 Forward Scattering.....	38
Figure 3.5 Backward Scattering .....	39
Figure 3.6 Sequential Pattern of Dark and Light Fringes at Crossing Volume .....	40
Figure 3.7 . Phase Shift Representation .....	41
Figure 3.8 MDG-100 Setup .....	47
Figure 3.9 Pointwise Measurements on Spray Cone .....	49
Figure 3.10 Axial Velocity Contour of Experiment 1 .....	49
Figure 3.11. Axial Velocity Plot of Experiment 1 .....	50
Figure 3.12 Radial Velocity of Experiment 1 .....	50
Figure 3.13. Sauter Mean Diameters for Experiment 1 .....	51
Figure 3.14 Axial Velocity Plots for Experiments 1,2 and 3 .....	52
Figure 3.15 Radial Velocity Plots for Experiments 1,2 and 3 .....	52
Figure 3.16 SMD Value Plots for Experiment 1,2 and 3 .....	53
Figure 3.17. Streamlines For Experiment 1,2 and 3 .....	53
Figure 3.18 Axial Velocity Plots for Experiment 10,11 and 12.....	55
Figure 3.19 Radial Velocity Plots for Experiment 10,11 and 12.....	55
Figure 3.20 SMD Values for Experiments for 10, 11 and 12 .....	56
Figure 3.21 Streamtraces for Experiment 10,11 and 12 .....	56

Figure 3.22 Axial Velocities for Experiments 1,4 and 7 .....	58
Figure 3.23 Radial Velocities for Experiment 1,4 and 7 .....	58
Figure 3.24 SMD Values for Experiments 1,4 and 7 .....	59
Figure 3.25 Spray Cone Angle Measurement with Shadowgraph Technique.....	60
Figure 3.26 Spray Cone Formation of Experiment 1,2 and 3.....	61
Figure 3.27 Spray Cone Formation of Experiment 10,11 and 12.....	61
Figure 3.28 Spray Cone Formation of Experiment 4,5,6 .....	62
Figure 3.29 Characteristic Number vs Spray Half Cone Angle .....	64
Figure 3.30 TMR versus Weber Number .....	64
Figure 3.31 Experimental and Estimated Spray Cone Angle Values .....	65
Figure A.1 Axial Velocities for Experiment 4,5 and 6.....	73
Figure A.2 Radial Velocities Experiments 4, 5 and 6 .....	74
Figure A.3 SMD Values for Experiment 4,5 and 6 .....	75
Figure A.4 Axial Velocities for Experiment 13 and 14.....	76
Figure A.5 Radial Velocities for Experiment 13 and 14 .....	77
Figure A.6 SMD Values For Experiment 13 and 14 .....	78
Figure A.7 Axial Velocities for Experiment 7,8 and 9.....	79
Figure A.8 Radial Velocites for Experiment 7,8 and 9 .....	80
Figure A.9. SMD Values for Experiment 7,8 and 9 .....	81
Figure A.10 Experiment 16,17 and 18.....	82
Figure A.11 Radial Velocities of Experiments 16,17 and 18.....	83
Figure A.12 SMD Values for Experiment 16,17 and 18 .....	84

## LIST OF ABBREVIATIONS

### ABBREVIATIONS

CFD	Computational Fluid Dynamics
GCH <sub>4</sub>	Gaseous Methane
LH <sub>2</sub>	Liquid Hydrogen
LO <sub>x</sub>	Liquid Oxygen
LPRE	Liquid Propellant Rocket Engine
MR	Ratio Of Oxidizer Momentum To Fuel Momentum
NASA	National Aeronautics And Space Administration
NASA CEA	Nasa Chemical Equilibrium Application
O/F	Ratio Of Oxidizer Mass Flow Rate To Fuel Mass Flow Rate
PDPA	Phase Doppler Particle Analyzer
SMD	Southern Mean Diameter
TMR	Total Momentum Ratio

## LIST OF SYMBOLS

### SYMBOLS

$C^*$	characteristic velocity
$D_{cp}$	central gap diameter
$D_{ip}$	inner body diameter
$D_p$	pintle support thickness
$D_t$	pintle tip diameter
$K_1$	first characteristic number
$K_2$	second characteristic number
$K_3$	third characteristic number
$L_{aod}$	actual opening distance
$L_{open}$	pintle tip angle
$L_{tod}$	tracing opening distance
$R_{cp}$	center post radius
$t_{ag}$	thickness of annual gap
$t_{pg}$	pintle gap thickness
$t_t$	tip thickness
$\alpha$	pintle angle
$\theta$	shadow angle
$C^*$	characteristic velocity

# CHAPTER 1

## INTRODUCTION

### 1.1. Motivation

Challenging dreams in space industry makes engineers more diligent. Launch vehicle is one of the primary components having a high cost, reducing the cost of engines will help a lot to space transportation. Liquid rocket engines (LRE) are favored for launch vehicles because of their reusability and high performance. Efficiency, stability and throttling are concerns of LRE and injectors are the main elements of combustion efficiency. However, many types of pintle injectors are used for throttling.

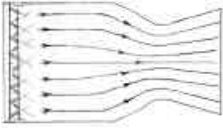
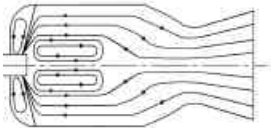
Injector is the main element in which propellants are supplied through to the combustion chamber. Main duty of an injector is to provide atomization of the fuel. Atomization quality is a key factor for minimizing the losses due to mixing at combustion chamber. Droplet size and the cone angle of sprays are determine this quality.

Pintle injector is one of the bipropellant injector type which has a varying injection area that provides throttling. At all thrust levels stable and efficient performances are expected. However, fixed area injectors experience some difficulties at lower thrust levels. Pintle injector overcomes the stability problem and also with varying injection area it controls the injection velocity hence the atomization characteristics. In addition to these capabilities, a pintle injector is able to inject propellants to the whole combustion chamber, which results in lighter injector plate compared to fixed area type injectors. This feature also satisfies to have cheaper LREs need.

### 1.1.1. Literature Review

A pintle injector is a type of injector which injects fuel and oxidizer through one or two controlled area. This control is provided by the injector components that changes the injection area which basically determines the injection velocity and affects the size of droplets in the combustion chamber. With its unique geometry, pintle injector provides a different flow field in the combustion chamber compared to typical injectors in the combustion chamber[1]. In his study, Gordon presented the differences between the typical liquid rocket engines and pintle engines and the table reproduced from their study is given as Table 1.1. Oxidizer or fuel is supplied through a coaxial pintle to the chamber via varying area which provides control on the thrust. The geometry is also easy to design and manufacture that allows rapid testing and evaluation. This brings out low development cost, an urgent need of the space industry. TRW company designed or tested a number of pintle engines, and they had more than 60 different pintle engine designs which have completed hot fire tests. These designs are utilized at different missions so that the designs are ranging from 5 lbf Brilliant Pebbles thruster to 650000 lbf LOX/LH2 engine to be tested at NASA Stennis Space Center. Among these designs, some had flight tests and according to Gordon 130 bipropellant engines have flown without a failure [1]. Moreover, Gordon states that combustion instability is not a concern of pintle engines, according to ground/flight tests over a range of 1:50000 in thrust and 1:250 chamber for 25 different propellant pairs [1]. Most popular one of these is Lunar Module Descent Engine for Apollo mission [2]. As shown in Figure 1.1 Oxidizer ( $N_2O_4$ ) goes through inner part of the injector and injected through variable area for throttling. For 1 to 10 throttling sleeve moves nearly 4 mm [2]. The difference between this injector and the injectors found on literature is instead of moving the pintle, a sleeve is used for altering/increasing the area. This provides the ability to control both the fuel ( $N_2H_4/UDMH$ ) injection area and oxidizer ( $N_2O_4$ ) injection area.

Table 1.1 Comparison Between Typical Liquid Rocket Engines and Pintle Engines (Reproduced from [1])

Parameter	 Chamber Flow Pattern in Typical Liquid Rocket	 Chamber Flow Pattern in TRW Pintle Rocket
<b>Injection Style</b>	Distributed from an injector plate	Single Element at the headend of the combustion chamber
<b>Fuel and oxidizer injection geometry</b>	Multiple intersecting or earring propellant streams; intersecting streams are of like or unlike propellants	Single annular outer sheet of one propellant impinges on (a) multiple radial “spokes” of other propellant, or (b) thin radial fan of other propellant
<b>Fuel and oxidizer collision geometry</b>	In plane immediately adjacent to injector face	In torus significantly offset from injector face
<b>Droplet trajectories</b>	Approximately axial down chamber	Initially at large angle to chamber axis
<b>Chamber recirculation</b>	None	Two major recirculation zones in chamber
<b>Droplet vaporization and combustion</b>	Proceed in planar fashion down chamber length	Proceed along axially symmetric, but highly non-planar, contours in chamber
<b>Secondary droplet breakup</b>	Comparatively small due to axial flow and homogeneous distribution	Comparatively large due to wall impingement and recirculation zones
<b>In passing through chamber, droplets see:</b>	Little “relative wind” away from injector face (pressure perturbation thus cause large change in energy release rate)	Large “relative wind” throughout chamber (pressure perturbations thus cause only small change in energy release rate)

<b>Energy release zone geometry</b>	Uniform and planar across chamber diameter (facilitates acoustically coupled combustion instability)	Radially-varying and canted down and across chamber together with stable zones having different gas properties (O/F, MW, gamma and T) serve to prevent acoustic instabilities
<b>Chamber for optimum combustion performance</b>	Is relatively short and has relatively small contraction ratio	Is relatively long and has relatively high contraction ratio
<b>Wall film cooling</b>	Established by separate injection ports	Established by pintle injector "tuning", eliminating need for separate ports
<b>Injection metering orifices</b>	Relatively small and contamination sensitive	Relatively large and insensitive to contamination

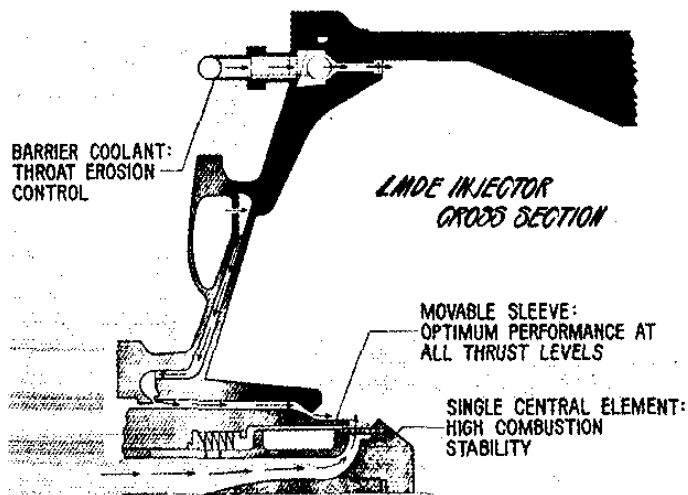


Figure 1.1 Lunar Module Descent Engine Pintle Injector [2]

In another study Gordon gave some important facts about Lunar Module Descent Engine (LMDE) [3]. One of the fact is that although LMDE is designed to 10:1 throttle, the engine design requirement was the throttle between 0-60% thrust level. However, they had development testing for over this range (0-100%) with no indication of combustion instability. In this study, he also listed the liquid rocket engines which are throttleable. Here, only the pintle engine ones are given in Table 1.2.

Table 1.2 Pintle Engines Manufactured (Reproduced from [3])

Names	Max Vacuum Thrust (lbf)	Throttle Range	Throttle Type	Propellant	Gordon's Comments
Lance Sustainer BC73-60	5000	357	Moveable Annular Pintle with Injection Pre-mix Chamber; Fuel Pressure-Actuated and Servovalve Controlled	IRFNA/UDMH	Larger throttle Range Demonstrated for Any Liquid propellant Rocket Engine
LMDE, TR200	10500	10	Cavitating Venturi Throttle Valve Linked to Variable Area, Single Element Pintle	N <sub>2</sub> O <sub>4</sub> /A-50	Pressure Fed Engine; A-50 includes 50% UDMH, 50% Hydrazine; 9850 lbf max thrust for flight engines

In their design Son et al. moved the pintle instead of the sleeve so that they controlled only the oxidizer area as shown in Figure 1.2 [4]. They had a cold test for simulating pintle injector for 500N LOX/Methane combustor. They defined their design parameters as  $D_{ob}$  (outer body diameter),  $D_{ib}$  (inner body diameter),  $D_{cg}$  (center gap diameter),  $D_{pr}$  (pintle rod diameter),  $D_{pt}$  (pintle tip diameter),  $\theta_{pt}$  (pintle tip angle),  $t_{pe}$  (pintle end thickness),  $t_{ann}$  (annular thickness) and  $L_{open}$  (pintle opening distance) as shown in Figure 1.2. Pintle tip angle is kept constant at  $40^\circ$  for all tested injectors. As stated in the introduction part, cone angle and the droplet size are two major concerns to have an efficient LRE. Son had an experimental setup including stroboscope and a high-resolution CMOS camera to measure cone angle. They also used a laser diffraction meter to measure Sauter mean diameters (SMDs). The schematic of the experimental setup is given in Figure 1.3. They defined a characteristic number for

the given geometry, and they presented empirical correlations for cone angle and SMDs.

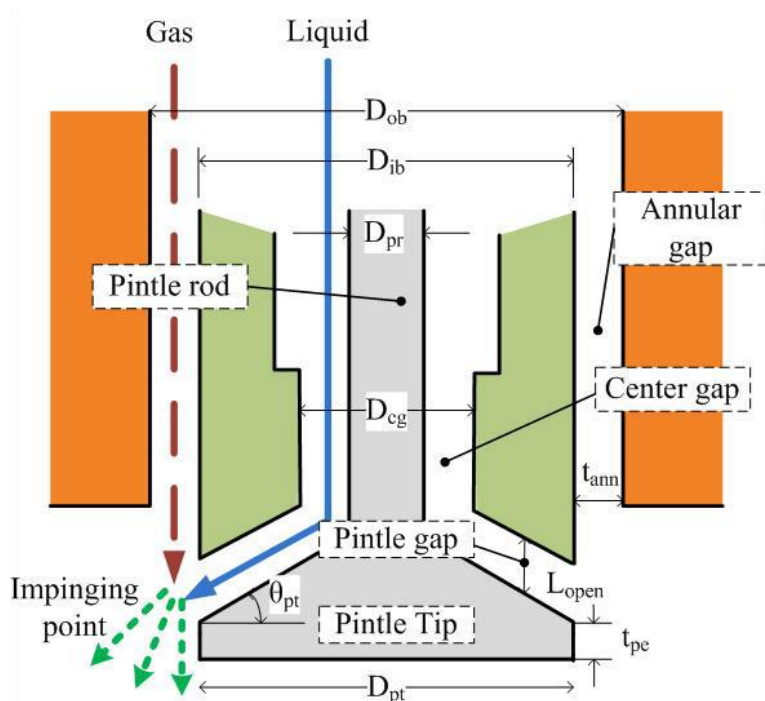


Figure 1.2. Base Design Geometry Son et al [4]

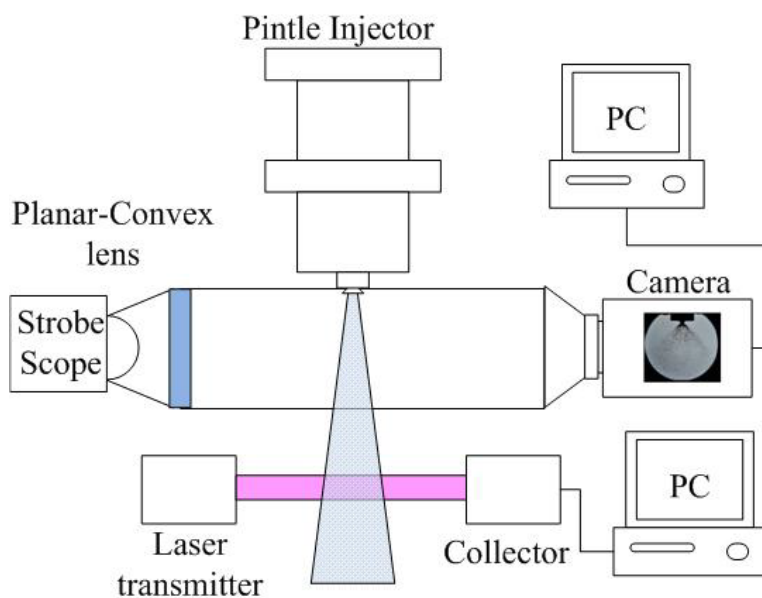


Figure 1.3 Experimental Setup of Son et al [4]

Another study of Son et al has also same base geometry; however, he changed some parameters from the previous study (Figure 1.4a) [5]. This time they have tried 3 different pintle tip angles at different opening distances. As the pintle opening area starts to be larger than the transition area (minimum orifice area inside the injector), pressure drop becomes independent from the pintle opening distance. There occurs a transition during the movement of the pintle, due to balance of the pintle opening area and minimum orifice area inside the injector. This transition area defines the range of the throttling for the considered pintle. Because of that reason they obtained geometrical formula for the varying area depending on the opening distance and the other geometrical parameters. They define this area as minimum orifice area ( $A_{min}$ ) and give the opening distance versus minimum orifice area in Figure 1.4b. As long as the calculated area is smaller than the annular area ( $A_{cg}$ ), moving pintle enables the throttling. On the contrary, if the area is greater than the annular area, it means that the mass flow rate is at its maximum and only the injection velocity can be changed by the increasing area.

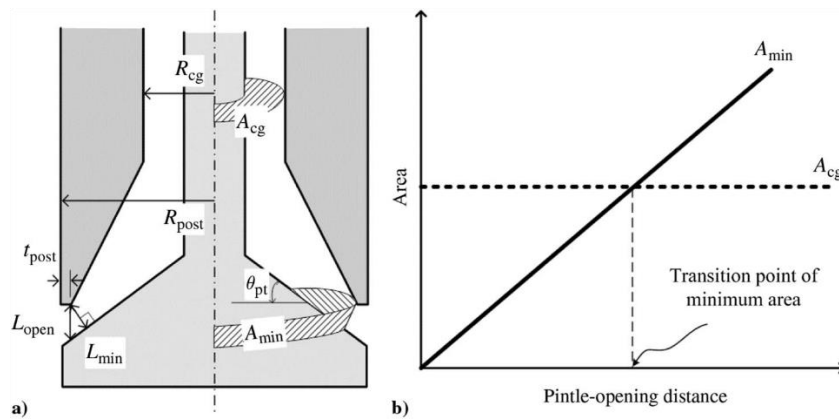


Figure 1.4 a) Base Geometry of the second work of Son et al [4] b) Pintle opening distance vs transition point [4]

They also included non-dimensional parameters such as new characteristic number  $K$  and Weber number to present the experiments they carried out [5]. In this study, Son et al defined the cone angle as the angle between horizontal line at the impinging point and the water jet at a distance of 50 mm which is equal to 6.25 times the post diameter

of pintle. It should be noted that in the previous work, the cone angle was defined as the angle between the axis and the water jet (Figure 1.5).

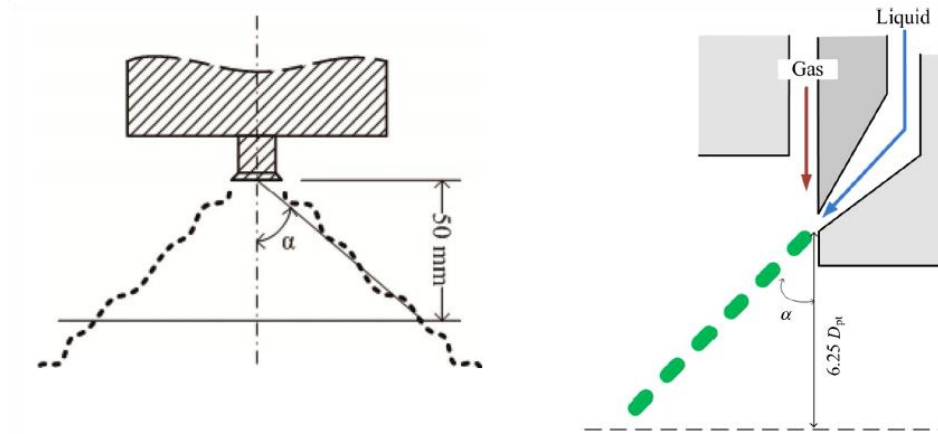


Figure 1.5 Cone Angle Defined by Son et al (on left [6], on right [5])

Son et al. conducted a numerical study on the combustion characteristics with a similar base geometry as shown in Figure 1.6 [6]. Although, it is stated that the same geometry with the previous studies has been used, the geometry in the numerical study is slightly different. The difference is a new parameter, center post radius, which is shown in Figure 1.7. As seen from the figure only the PI-4 has the same base geometry with the previously discussed studies. Pintle tip angle is selected  $40^\circ$  for all given geometries. Center post radius ( $R_{cp}$ ) and pintle opening distance ( $L_{open}$ ) are two comparison parameter. Analysis are performed with FLUENT software and standard  $k-\epsilon$  model is used with 2D axisymmetric condition. Adiabatic wall is assumed at combustion chamber wall and nozzle and a constant temperature of 600 K is applied as the boundary condition. The cases and the conditions are given in Table 1.3 and Table 1.4. The renewed geometry ( $L_{cp}$ ) in the center post radius brings a new point of view to the fuel centered pintle injector for these types of geometries (Figure 1.6). In the numerical the analysis, a new recirculation area just at the end of the annular gap is observed due to the difference between  $D_{cp}$  and  $D_{ib}$  (inner body diameter). This recirculation may lead to high temperatures at pintle tip as stated in Figure 1.8 which may lead to thermal problems like dilatation [6].

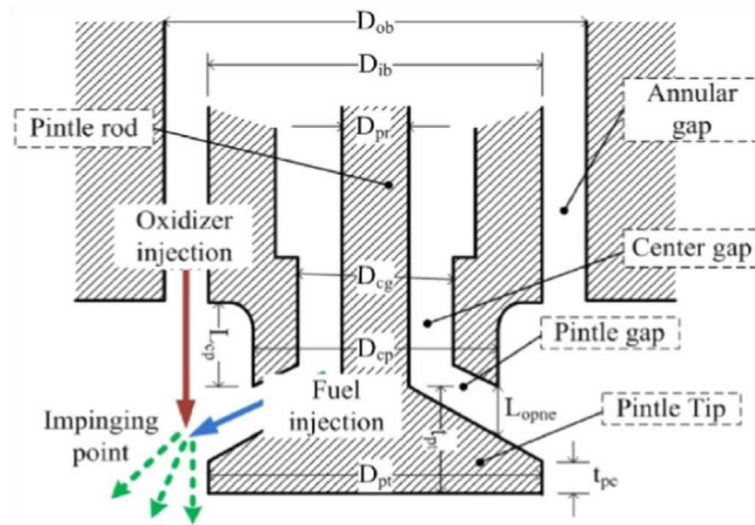


Figure 1.6 Base Geometry of Numerical work of Sun et al [7]

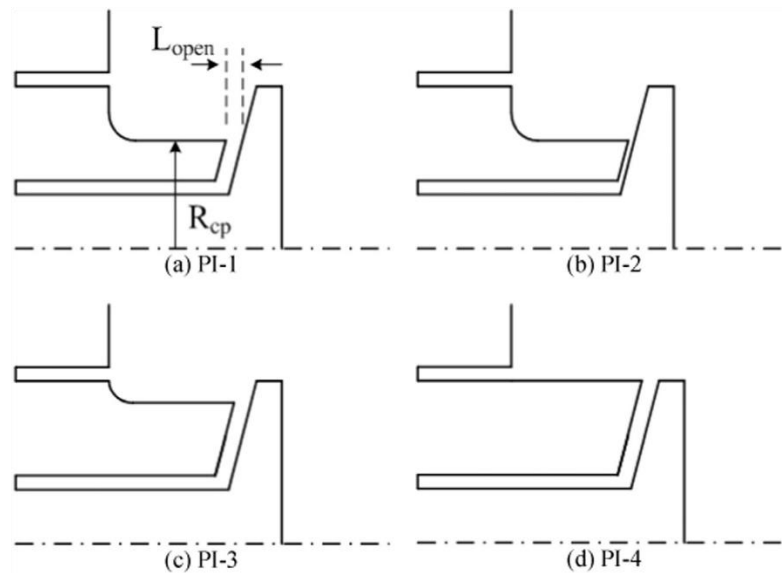


Figure 1.7 4 Different geometries studied by Son et al [7]

Table 1.3 Geometric Inputs for the Analysis Performed by Son et al (Reproduced from Ref. [7])

Geometry in Figure 1.7	Center Post Radius [mm]	Pintle Opening Distance [mm]	CH4 Injecting Area [mm <sup>2</sup> ]
PI-1	4	0.6	13.4
PI-2	4	0.2	4.55
PI-3	5	0.6	16.84
PI-4	6	0.6	20.29

Table 1.4 Mass Flow Rates and Targeted Chamber Pressures for the Analysis Performed by Son et al. (Reproduced from Ref [7])

	Geometry at Figure 1.8	Calculated Chamber Pressure [bar]	Mass Flow Rate [kg/s]	
			CH <sub>4</sub>	O <sub>2</sub>
Analysis 1	PI-1	20	0.01770	0.07100
Analysis 2	PI-1	10	0.00887	0.03550
Analysis 3	PI-2	10	0.00887	0.03550
Analysis 4	PI-3	20	0.01770	0.07100
Analysis 5	PI-4	20	0.01770	0.07100

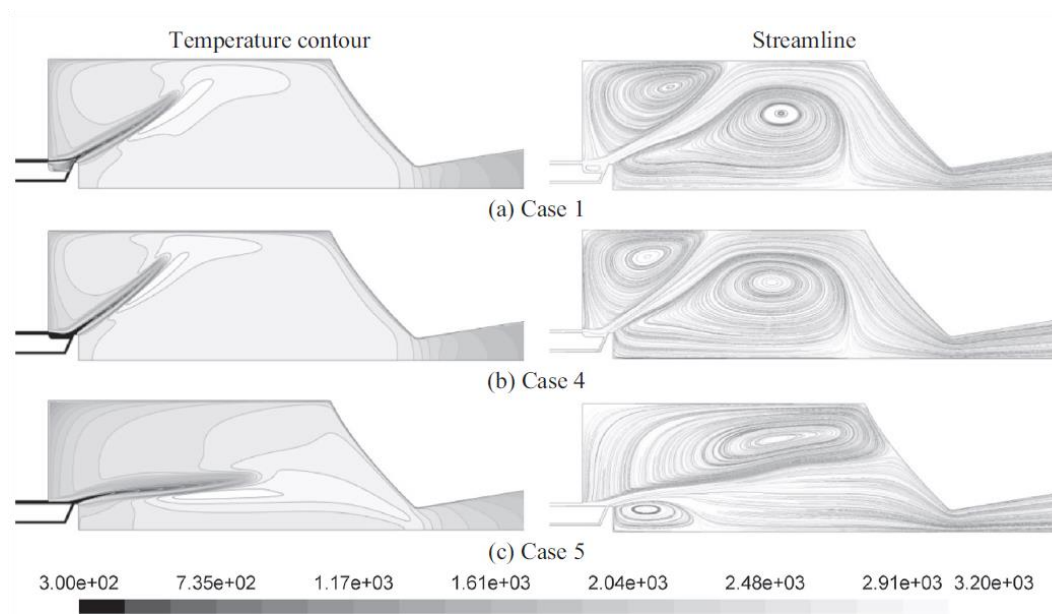


Figure 1.8 Comparison of Post Center Radius Effect From the Study of Son et al [7]

Son et al. studied air and water as simulants of LOX and GCH<sub>4</sub>. They applied 3 different non-dimensional numbers in their assessments which are Weber, Reynolds and characteristic number K (three different numbers at three different works). Characteristic numbers are defined with 3 following equations:

$$K_1 = \frac{V_{gas} t_{ann}}{V_{liq} L_{open}} \quad (1)$$

$$K_2 = \frac{MR \cdot Re_{liq}}{Re_{gas}} \quad (2)$$

$$K_3 = \frac{\left(\frac{\rho_{gas}}{\rho_{air@atm}}\right)^{0.5} V_{gas} t_{ann}}{\left(\frac{\rho_{liq}}{\rho_{water}}\right)^{0.5} V_{liq} L_{open}} \quad (3)$$

In these 3 equations ‘liq’ and ‘gas’ subscripts stands for LOX and GCH<sub>4</sub>. These non-dimensional numbers are revealed to correlate geometrical pintle parameters to SMD and spray cone angles. MR stands for momentum ratio, which is the ratio between gas and liquid momentum, and Re stands for Reynolds number. First two of these equations are achieved from water-air atmospheric condition cold flow tests which do not include the effect of the density change, on the contrary third one includes the effect of density of the working fluid. All these characteristics numbers are tested with number of cold flow test procedure. These parameters are utilized to predict the cone angle and particle size distribution of the sprays at special empirical correlations driven for this injector geometry. The experiment results conducted are shown in Figure 1.9, Figure 1.10 and Figure 1.11. In these figures characteristic number is K<sub>1</sub> and increasing characteristic number decreases the spray cone angle, moreover particle size decreases within increasing Weber. One can observe this phenomenon in Figure 1.11. In addition to that, it is seen that increasing the pintle opening distance corresponds to particle size decrease with the corresponding velocity ratios in Figure 1.11.

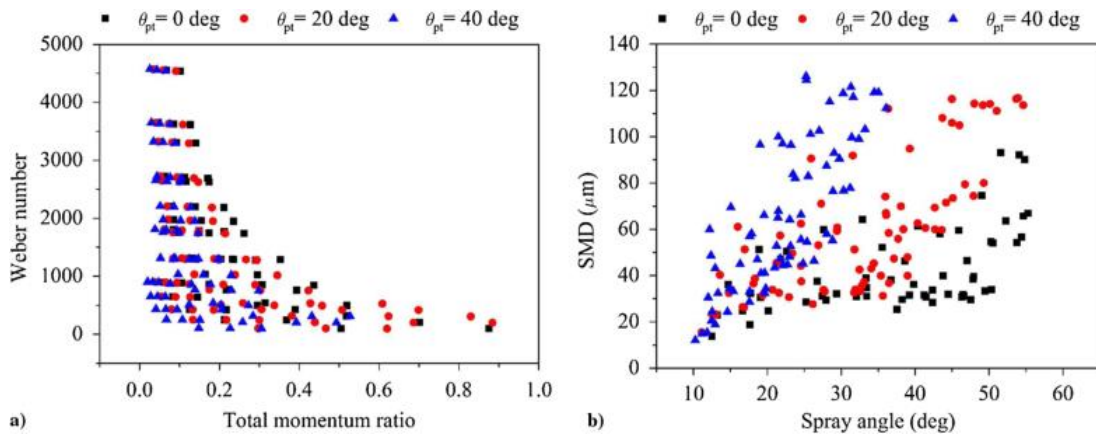


Figure 1.9. Weber Number-Total Momentum Ratio Relation for 3 Different Pintle Tip Angles [5]

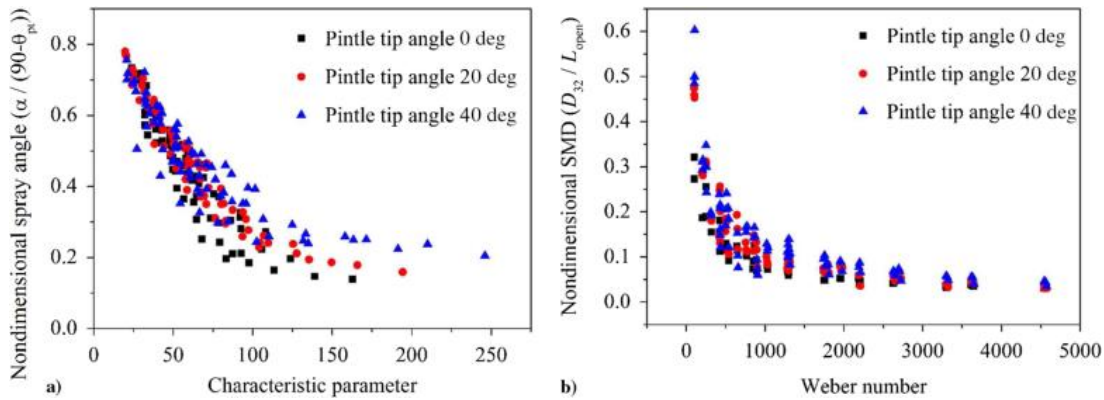


Figure 1.10 Spray Angle-Characteristic Number Relation for 3 Different Pintle Tip Angles [5]

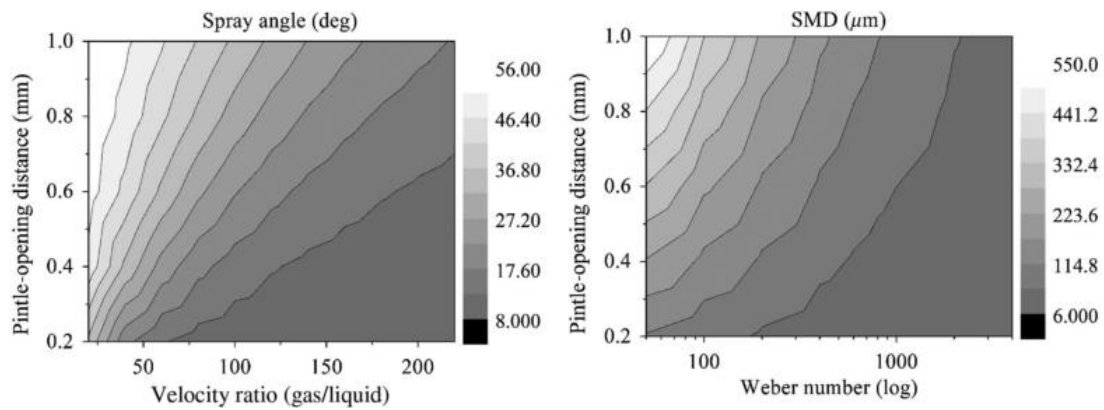


Figure 1.11. Velocity Ratios of Son's Study [5]

Third correlation ( $K_3$ ) is obtained by cryogenic spray study with the same geometry used in reference [5] in which first correlation ( $K_1$ ) is obtained. In this test,  $\text{LN}_2$  and  $\text{GN}_2$  are fed to a high-pressure chamber and shadowgraph images are captured. Spray

cone angles are measured from the captured high-speed camera images. The comparison with atmospheric and high-pressure chamber experiments and the predictions for spray cone angles are presented in Figure 1.12. These measurements include both previous and current studies' measurements, transparent points indicate that these are from the previous studies which are conducted under atmospheric conditions. However, for this study high-pressure chamber environment is the case which effects the spray cone angle also because the density of the working gas differs tremendously. Under these conditions, to predict spray half cone angle, another characteristic number,  $K_3$ , is proposed which includes density effects. This non-dimensional number predicts spray half cone angle better than  $K_1$  and  $K_2$  as stated by Lee [15] and the estimation and experimental results are given in Figure 1.12 where TMR stands for total momentum ratio.

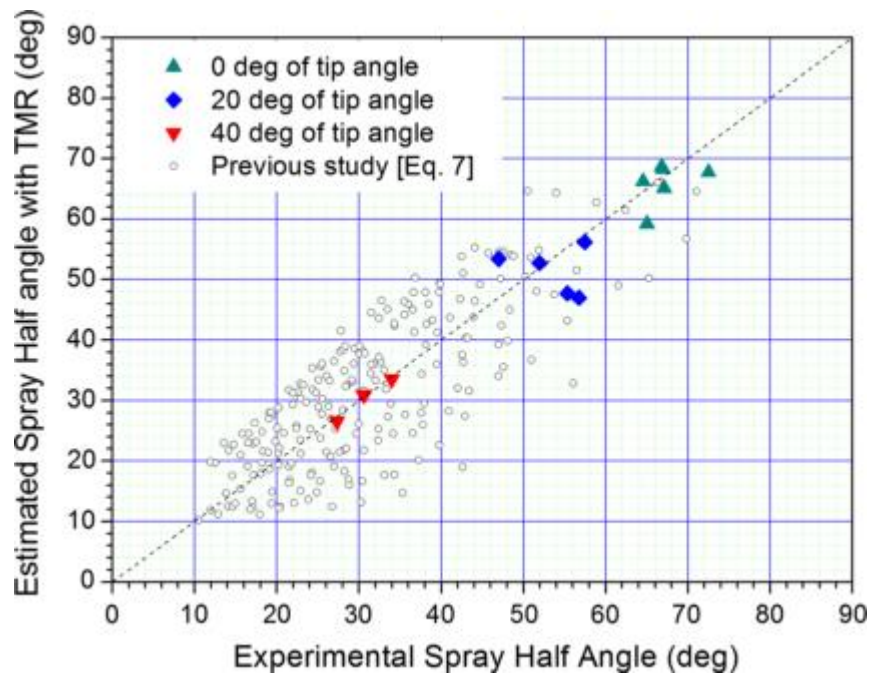


Figure 1.12 Comparison with atmospheric tests [15]

Badard worked on throttleable LOX-LCH<sub>4</sub> pintle engine and they had a chance to conduct hot fire tests. The design parameters are 21.7 bar chamber pressure, 5785-18690 N thrust and some hardware limitations for weight, size etc [7]. The test is based on a different geometry (Figure 1.13) compared with the Son's study [5]. It has a

shower head type injector and the oxidizer (LOX) is supplied through the pintle instead of the supply of the oxidizer over the pintle. At the tip of the pintle, there exists a replaceable component which is a slotted ring. This ring adjusts the orifice area with different slot sizes for each experiment. Each ring satisfy a throttling level for each experiment (Figure 1.14) . An important contribution of the author is solution of the uniformity problem of the flow after the reservoir. They stated that non-uniform flow may occur depending on the reservoir geometry of the injector. In their study, they have faced with the uniformity problems at the annular gap flow in the initial designs (Figure 1.15). Modifying the reservoir geometry, they obtained uniformly distributed flow. The flow observations is presented in Figure 1.15, moreover; the internal manifold geometry is given both in Figure 1.13 and Figure 1.15.

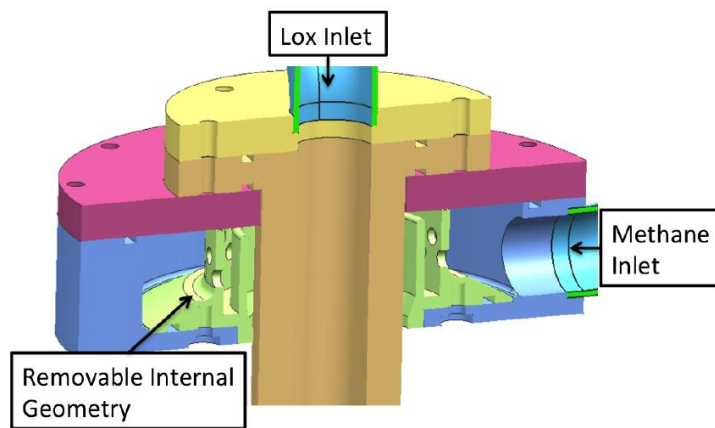


Figure 1.13. Base Geometry of Badard et al [8]



Figure 1.14 Components of Pintle Injector Designed by Badard et al [8]



Figure 1.15. Uniformity of the Jet Introduced by Bedard [8]

In their study Cheng et al. stated that there is a lack of relations for spray cone angle prediction on pintle injectors which is a vital parameter for the combustion [8]. For that reason, they developed a theoretical correlation for the prediction of the cone angle for liquid-liquid pintle injectors. They validated their correlation by numerical simulations, experiments and also with the other studies. Their main assumptions for the method are incompressible flow, velocity vectors are normal to both inlet and outlets, no surface tension, no heat transfer (such that no phase change) and no body force. Two control volumes are considered for two propellants and an interaction

between them is investigated as shown in Figure 1.16. They found out that the cone angle is dependent on TMR (total momentum ratio) as indicated by Equation (4). They used VOF (volume of fluid) method for CFD (Computational Fluid Dynamics) simulations to evaluate this theoretical correlation. They have selected water and air as simulants in their studies. They also conducted experiments to compare their method. They captured images by a high-speed camera with backlit photography technique. Theoretical model, simulations and experiments for obtaining cone angle are compared in Figure 1.17.

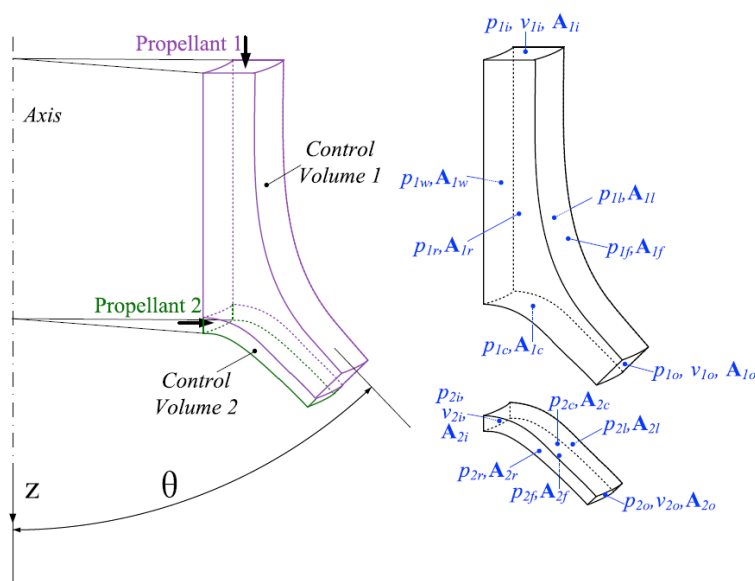


Figure 1.16. Momentum Equation Applied Control Volumes [9]

$$\cos(\theta) = \frac{1}{1 + TMR} \quad (4)$$

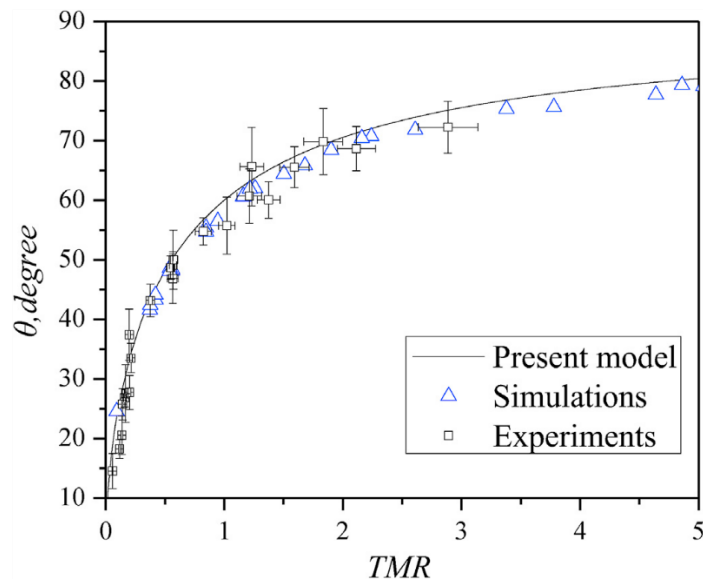


Figure 1.17 Comparison of 3 Ways to Determine Cone Angle

Sakaki et al. stated that literature is not sufficient to propose a well-defined flame and spray structure for hot fire conditions because of difficulties in optical measurements [9]. They conducted experiments for ethanol/LOX combustion in a rectangular combustor with planar pintle injector. The details of the injector are given in Figure 1.19 where ST1 to ST8 are the thermocouple numbers. They conducted 4 different experiments including fuel-centered and oxidizer-centered pintle injectors. A fuel-centered pintle injector used in the experiment is given in Figure 1.19 where the total momentum ratio (TMR) is 0.49, chamber pressure is 3.5 bar and O/F ratio is 1.4. In another study Sakaki et al. stated that  $C^*$  efficiency is affected by TMR (more effective on oxidizer-centered pintle injectors), as TMR is increased,  $C^*$  decreases [10].

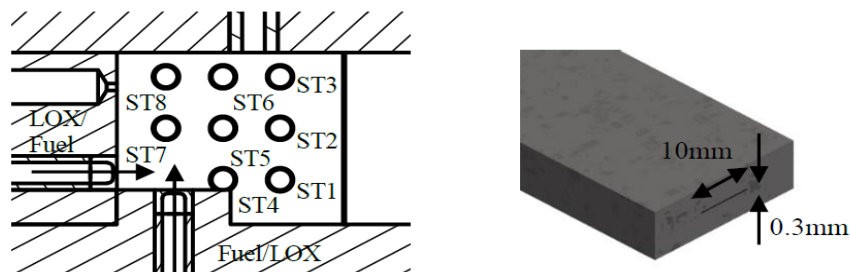


Figure 1.18 Injector Configuration of Reference [9]

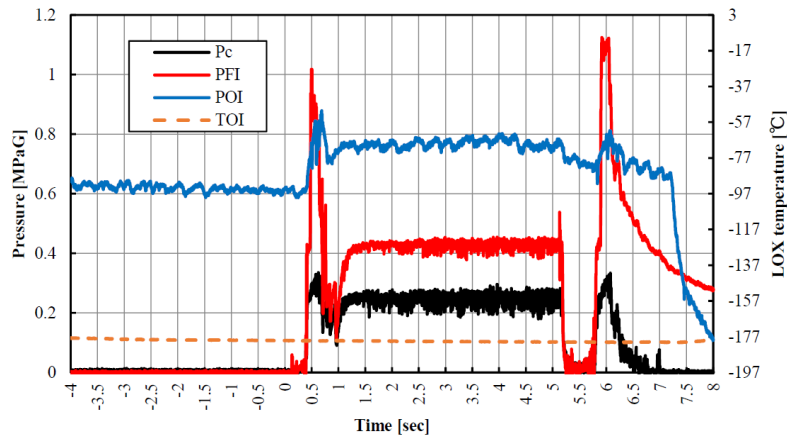


Figure 1.19 Fuel-Centered Pintle Injector Hot Fire Test Done by Sakaki (Chamber Pressure, PFI: Fuel injection pressure, POI: Oxidizer injection pressure, TOI: Oxidizer injection temperature) [10]

Another hot fire test is accomplished by TRW for low cost pintle engine (LCPE), which is a 650000 lbf LOX/LH<sub>2</sub> engine [11]. It is stated that manufacturing costs for the previous missions are ranging from \$77/lbf to 175\$/lbf and they aimed to lower the cost of manufacturing further. Thus, pintle engines are conceptual candidates. They designed and manufactured a 650 Klbf LOX/LH<sub>2</sub> pintle engine to validate the cost analysis. The injector has 5 components and these components are easy to fabricate compared to the multiple-orifice doublet triplet or multi-element coaxial injectors. LOX is fed from the center and it is injected radially from the holes at the tip. LH<sub>2</sub>, which is fed from an annular gap, meets with the LOX impingement at the pintle tip. The injector technical drawing of the injector and the injector itself are given in Figure 1.20.

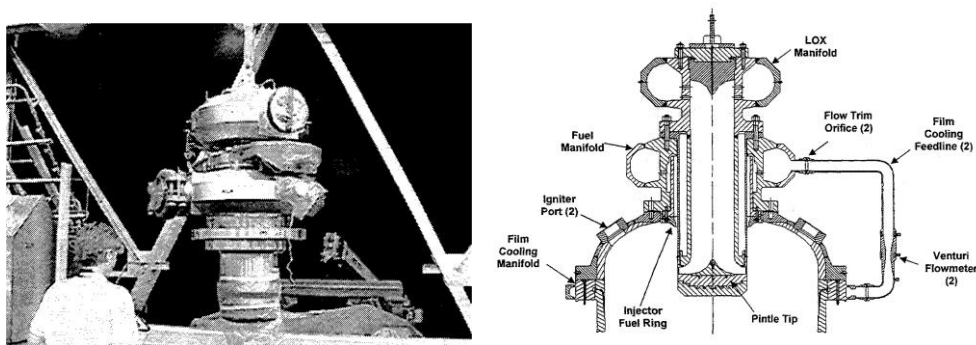


Figure 1.20 Technical Drawing and Injector Itself of LCPE [11]

Gromski et al studied TR202 LOX/LH<sub>2</sub> deep throttling engine which is another program for developing the pintle technology [12]. They manufactured a test stand for pintle injectors for easy switching to the other pintle configurations to test different throttle levels. The design does not contain a linear actuator to move the pintle or any other component to throttle. The dimensions of the shower head style injector assembly are 18 in x 18 in x 9.5 in and has 200 lbs weight. All the tests were successful for 10:1 throttle ratio (75 %-7.5 % of full power) and 98.6 C\* efficiency is obtained at 75 % thrust (6545 lbf).]

In this chapter, numerical and experimental work conducted for several pintle injector types are introduced briefly. To sum up, cold flow experiments are necessary to investigate the injector characteristics and particle size and spray cone angle are the key factors on the performance of the injector which are simply determined by geometrical parameters of the injector. Previous works are performed to measure spray cone angle and particle sizes of the droplets. Moreover, empirical correlations and non-dimensional parameters are proposed to predict spray cone angle and particle sizes. Although it is not in the scope of this work, hot flow tests are discussed to deeper understanding of the pintle injector challenges.

With this work, a new experimental approach to measure droplet sizes is presented which is Phase Doppler Particle Analyzer (PDPA). Moreover, velocity field and particle size distributions are presented. 6 different continuous pintle injectors are investigated with 3 different pintle tip angle and 2 different annular gaps.



## CHAPTER 2

### DESIGN PROCEDURE

#### 2.1. Introduction

In this study, a bipropellant oxidizer centered pintle injector is designed with the requirements 750 N thrust, 3:1 throttle ability. While the fuel injection area is kept constant, the flow injection area of the oxidizer is variable in order to have a simple mechanism.

The design consists of two main regions. First is the flow region, which is near the outlet of the injector, and it determines the flow characteristics of the spray (droplet size, cone angle etc.). This region will be referred to as the outlet region in the remaining part of this study. The second region is the inlet of the injector which determines the uniformity of the flow at the outlet region. This portion will be named as inner geometry design in the remaining part of this study.

The first part to be designed is the outlet region since the mission requirements of the LRE is totally dependent on the geometry of this region. This portion directly affects the spray cone angle and droplet formation thus the design starts by the defining the geometrical parameters of the outlet region. However, to have a uniform flow at the outlet region, design of the inner geometry should be designed properly. Although, the main characteristics of the combustion chamber is determined by the outlet region, in order to have a uniform flow there, the second region should also be designed carefully. The flow passing through inner geometry is directly injected from the outlet region. Thus, flow through the outlet region can be torsional if the inner geometry is not designed properly.

## 2.2. Design of Outlet Region

As discussed in Section 1.1.1 there are several types of pintle injector. For this work, the outlet region geometry is selected similar to Son's geometry to have throttle capability as shown in Figure 2.1 [4]. Geometrical parameters are listed in Table 2.1:

Table 2.1. Enter the Table Caption here

Parameter Name	Symbol	Type of Parameter
Pintle support thickness	$D_p$	Input
Pintle tip diameter	$D_t$	Input
Actual opening distance	$L_{aod}$	Output
Tracing opening distance	$L_{tod}$	Output
Thickness of annular gap	$t_{ag}$	Input/Output (Iterative)
Pintle gap thickness	$t_{pg}$	Input
Pintle angle	$\alpha$	Input
Shadow angle	$\theta$	Input
Tip thickness	$t_t$	Input

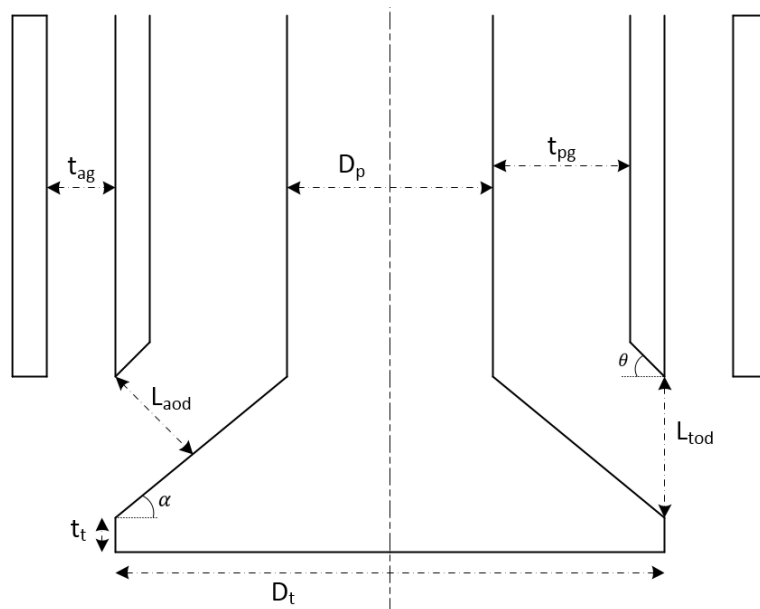


Figure 2.1 Base Geometry for the Design

To start the design, the mission requirements are to be used as input parameters. Thrust, chamber pressure, propellants, oxidizer and fuel injection temperatures, throttle capability, O/F ratio range to be observed are given as inputs. Thickness of annular gap and actual opening distance, which are given in Figure 2.1, are the output of the design code. On the other hand,  $D_p$ ,  $D_t$ ,  $t_{pg}$ ,  $\alpha$  and  $\theta$  are given as inputs to the code.

Although the only option suitable for the period of the study is cold flow testing, the design procedure is carried out for the real condition. The mission requirement is to design a 750 N pintle injector with liquid oxygen (LOX) and gaseous methane (CH<sub>4</sub>) as oxidizer and fuel respectively. Theoretical calculations are done according to real propellants, LOX and gaseous CH<sub>4</sub>. The design starts with the calculation of the mass flow rates of the propellants. For this purpose, Eq. (5) is used to obtain mass flow rates,

$$T = \dot{m}I_{sp}g \quad (5)$$

where T stands for thrust,  $\dot{m}$  stands for total mass flow rate of propellants,  $I_{sp}$  stands for specific impulse and g stands for gravitational acceleration.

Thrust is the design parameter, and  $I_{sp}$  should be calculated. NASA Chemical Equilibrium Application (NASA CEA) is used to calculate corresponding  $I_{sp}$ . However, application requires chamber pressure and oxidizer/fuel (O/F) ratio as inputs. The mass flow rate of methane is chosen to be constant for the hot flow experimental conditions. Moreover, LOX mass flow rate is taken to be equal to gaseous CH<sub>4</sub> mass flow rate at the start of the hot fire test which is a required condition for the hot flow experiment. The flow rate of LOX increases at higher throttle levels. As the throttling level increases, pintle opening distance and mass flow rate of the oxidizer are also increased. This corresponds to higher O/F ratios for higher thrust levels in the injector. The steps for the design are as follow:

1. The design starts by choosing a chamber pressure and O/F ratio at lowest thrust level. At this level, expansion ratio is chosen to be ideally expanded to sea level and NASA CEA is used for this specific point.
2. Characteristic velocity ( $C^*$ ), thrust coefficients ( $C_f$ ) and specific impulse ( $I_{sp}$ ) are calculated by NASA CEA at the lowest thrust level where characteristic velocity is defined as combustion efficiency and thrust coefficient is defined as the nozzle performance coefficient.
3. Required O/F ratios (by mission requirement) for all thrust levels are supplied as inputs at the same chamber pressure of the lowest thrust level.
4.  $C^*$  values are calculated for the 3<sup>rd</sup> step at the same chamber pressure value of the lower thrust level.

The calculations up to this step are summarized in Table 2.2. Here the O/F ratio and pressure chamber are the inputs for NASA CEA and  $C^*$  is obtained for the corresponding O/F ratios.

*Table 2.2. Tabulated Version of Step 4*

O/F Ratio	$P_{\text{chamber}}$ [bar]	$C^*$ Obtained at the Lowest Thrust Level [m/s]
1	20	1346
2	20	1784
3	20	1815
4	20	1727

5. Obtained  $C^*$  and  $I_{sp}$  values are used with the corresponding O/F ratio to calculate the real chamber pressure. For this step, the ratio between the mass flow rate of the lower thrust level and corresponding mass flow rate is known because O/F ratio is an input and mass flow rate of fuel is taken as constant (Table 2.2). To calculate real chamber pressure, the following relation is used:

$$\frac{C_1^*}{C_2^*} \equiv \frac{\frac{P_{c1} A_t}{\dot{m}_1}}{\frac{P_{c2} A_t}{\dot{m}_2}} \quad (6)$$

6. After completing the previous step for all thrust levels, the real chamber pressures at these levels are calculated. These calculated chamber pressures are again used in NASA CEA as inputs and corresponding  $C^*$ ,  $C_f$ ,  $I_{sp}$  values are compared with the ones that are found in the first two steps. If the difference is more than 2%, another chamber pressure for thrust level is chosen for lowest thrust level to have design and the calculations start with the first step again.
7. Highest thrust level is given as the input. Mass flow rate and throat area is calculated with following relations for all thrust levels.

$$T = \dot{m} I_{sp} g \quad (7)$$

$$T = P_c C_f A_t \quad (8)$$

8. From O/F ratio for highest thrust level, mass flow rates for LOX and GCH<sub>4</sub> is calculated.
9. Annular gap thickness is increased until the velocity of GCH<sub>4</sub> at annular gap is less than the speed of sound.
10. Tracing opening distance ( $L_{tod}$ ) is calculated using the Eq. (9) where K is the characteristic number defined by Eq. (1) at Section 1.1.1 [5].

$$L_{tod} = \frac{\dot{m}_{oxidizer}}{\dot{m}_{fuel}} K \left( \frac{t_{ag}}{\rho_{liq} A_t R_{gas} T_{gas}} \right) \left( \frac{\mu_{liq}}{\mu_{gas}} \right) T \quad (9)$$

11. Tip diameter and pintle angle are given as initial guesses to calculate TMR by Eq. (10).

$$TMR = \frac{\dot{m}_{water} V_{water} \cos(\alpha)}{\dot{m}_{air} V_{air} + \dot{m}_{water} V_{water} \sin(\alpha)} \quad (10)$$

Six different injector types are designed following these steps for 2 different annular gaps and 3 different pintle angles. It can be observed that, determination of  $L_{tod}$  is independent of the pintle angle. However, it is dependent to annular gap thickness. For this reason, to design comparable injectors, characteristic number  $K$  (Eq. (3)) is adjusted in order to have the same  $L_{tod}$ . Annular gap thicknesses are chosen as 0.5 mm and 1 mm and corresponding characteristic numbers are chosen as 0.25 and 0.13, respectively. These values are chosen because at full thrust position of the injector,  $L_{tod}$  is desired to be kept at 0.5 mm which is related to inner geometry as will be discussed in following section. At the end the design has the same pintle opening distance position for all injector types and the design points are tabulated in Table 2.3.

Table 2.3 LOX and GCH<sub>4</sub> Mass Flow Rates and Corresponding Pintle Tracing Distance

O/F Ratio	Chamber Pressure Obtained by Step 1 [bar]	C* [m/s]	Cf	Thrust [N]	Fuel Mass Flow Rate [kg/s]	Oxidizer Mass Flow Rate [kg/s]	Pintle Tracing Distance [mm]
1	20.00	1346.0	1.51	232.27	0.0571	0.0571	0.04
2	39.76	1787.3	1.51	461.79	0.0568	0.113	0.15
3	53.93	1839.1	1.52	630.57	0.0564	0.169	0.32
4	64.15	1756.8	1.52	750.00	0.0562	0.22	0.50

### 2.3. Design of the Inner Geometry

Inner geometry has an important role to obtain the uniform flow conditions at the outlet region,. The location of the support of the pintle shaft often creates an

asymmetric flow condition because flow can only enter the reservoir from sides (perpendicular to shaft direction) instead of being in the direction of the shaft. The support of the shaft is generally placed at the center and this creates an asymmetric flow condition for the oxidizer. Similar problem also occurs for the fuel part. Since the fuel part mechanically covers the outer side of the oxidizer, it is not possible to design an inlet in the same direction with the outlet flow causing asymmetrical flow. Bedard et al. faced with a similar problem and they tried 3 different configurations to obtain axisymmetric flow as shown in Figure 1.13 and Figure 1.15 [7]. In this study, the inner geometry is obtained by experimenting several options. In this section 3 different inner geometry design types, which are the reservoir design, direct flow passage and moveable mechanism, are considered. For the first two of these only oxidizer flow is investigated and the design of inner geometry for fuel supply has not changed until uniform flow is satisfied for oxidizer flow. Finally, for the moveable mechanism both fuel and oxidizer inner geometry has been changed. All the experiments for uniformity analysis are done with water even for the fuel inlets water is supplied instead of air. It is because water flow is easy to visualize at the outlet region.

### **2.3.1. Alternative Design 1**

It is the simplest design compared to the others due to its easier production and also it does not include complex parts to assemble. The design is shown in Figure 2.2 where dark blue represents water (oxidizer) and light blue represents air (fuel). As seen from the figure, pintle is mounted far from the outlet of the injector, which makes this design dependent on the mechanical tolerances. The longer the length of the shaft, the more is the bending at the outlet region of the pintle. This bending at the tip of the pintle creates problems like fuel flow crossing the pintle tip instead of liquid sheet which is an undesired situation. Even if the mechanical tolerances are in the accepted and the bending problem has been solved, still the flow characteristics near the pintle tip is not acceptable. Water is supplied through inlets, which are perpendicular to the direction of the flow, causes a torsional flow phenomenon at the outlet region and through the

center gap region which is shown in Figure 2.3. Water is supplied without air to visualize the flow and the result is not satisfactory which can be observed by the figure. Because of that, this alternative design is not used for the experiments to measure spray cone angle and particle size of the droplets.

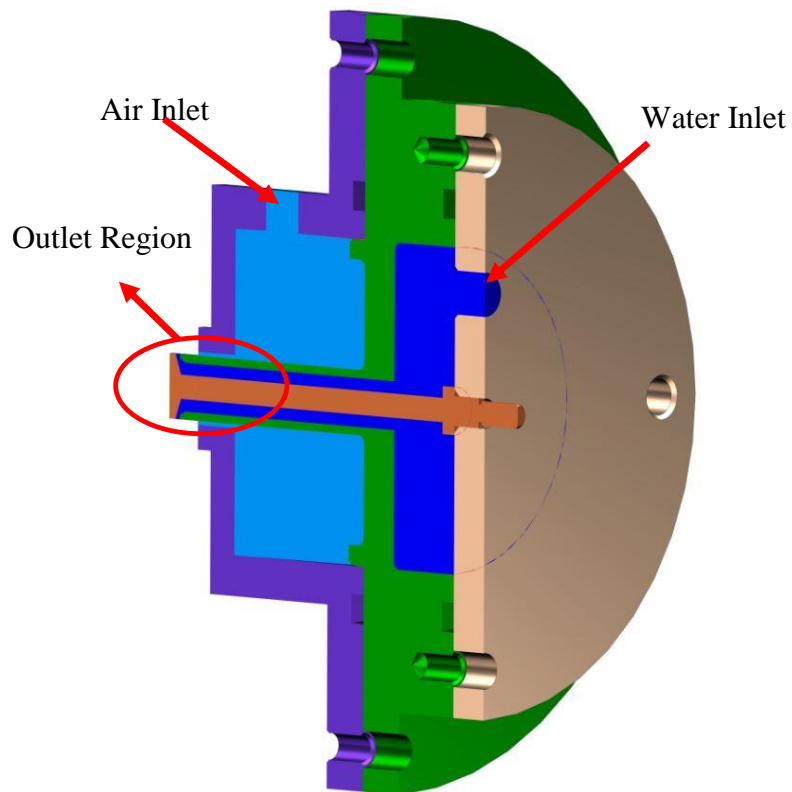


*Figure 2.2 First Alternative Design for Inner Geometry*



*Figure 2.3. Water Flow at Oxidizer Passage for First Alternative Design*

### **2.3.2. Alternative Design II**

This design is created to eliminate the bending problems faced in the reservoir design. The type and the location of the support have changed. The design is shown in Figure 2.4, dark blue represents water (oxidizer) and light blue represents air (fuel). Since, the support is closer to the pintle tip and longer than the previous one, bending problem is solved. Support as given with Figure 2.5 extends along the flow direction for 2 cm. This design is satisfactory for mechanical concerns; however, it is observed that the support geometry disturbs the flow at the inner geometry and creates vibration during the experiments. This vibration effected the flow uniformity at outlet region and even the spray cone orientation is affected from the vibrations. Thus, this inner geometry design is also not accepted as suitable for the spray cone, particle size and velocity measurements.

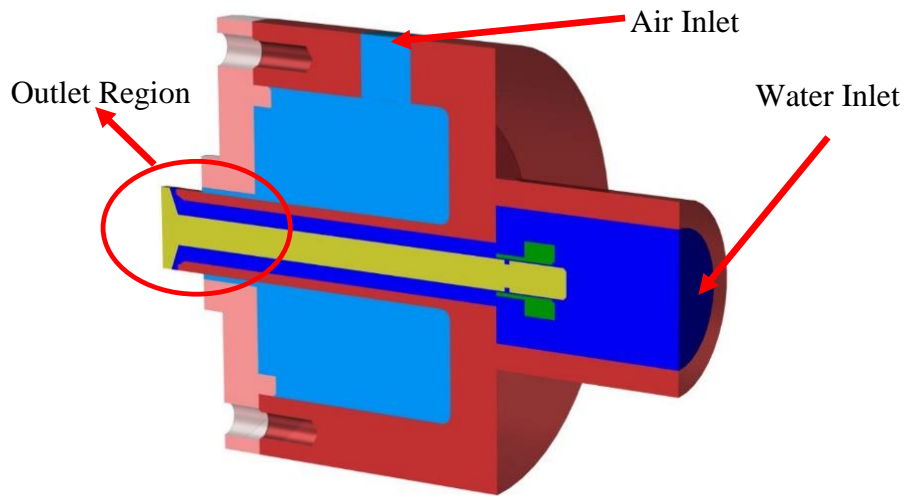


Figure 2.4. Second Alternative Design (Direct Flow Passage)

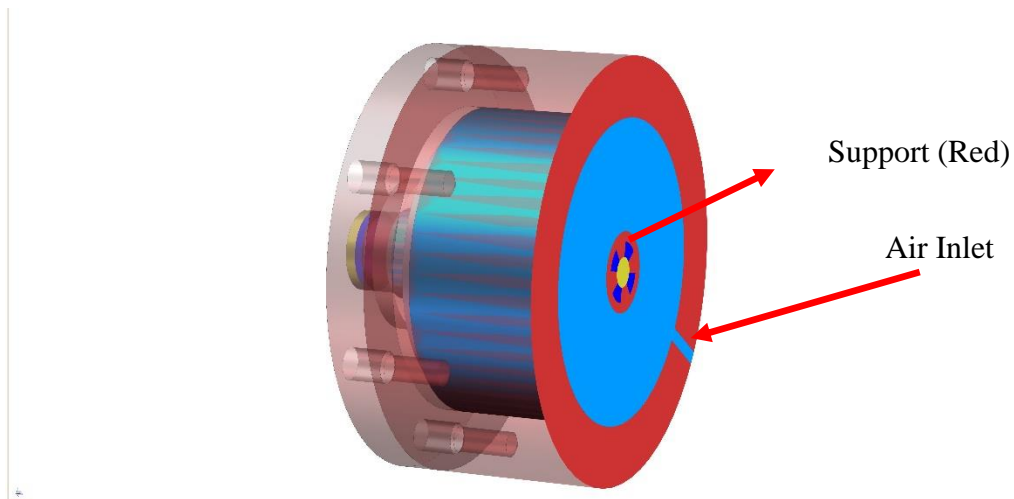
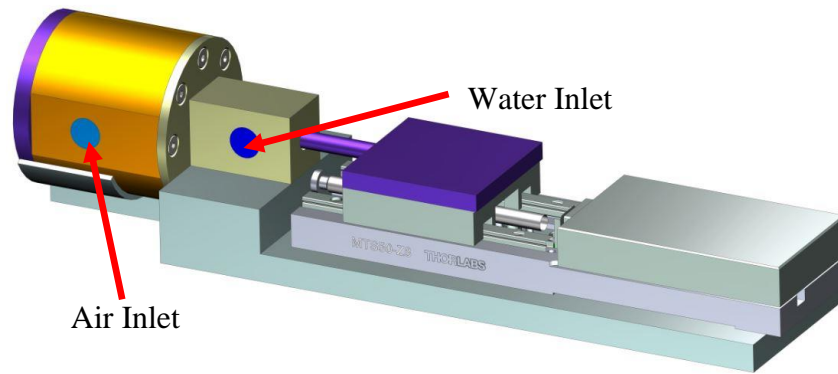


Figure 2.5. Second Alternative Design from Another Cross Section

### 2.3.3. Moveable Mechanism

This design is chosen as the final design and it is the only design tested with PDPA system and shadowgraph technique. Here, the main problem of pintle bending is solved with two mountings at two sections as shown in Figure 2.6. Again dark blue represents water (oxidizer) and light blue represents air (fuel). These two mountings are not only for supporting the shaft but also used for stabilizing the torsional flow.

Dimensions of the holes at the mountings are chosen according to manufacturing limits. However, diameters are designed to be as large as possible for easy manufacturing.



*Figure 2.6 Moveable Mechanism with Linear Actuator*

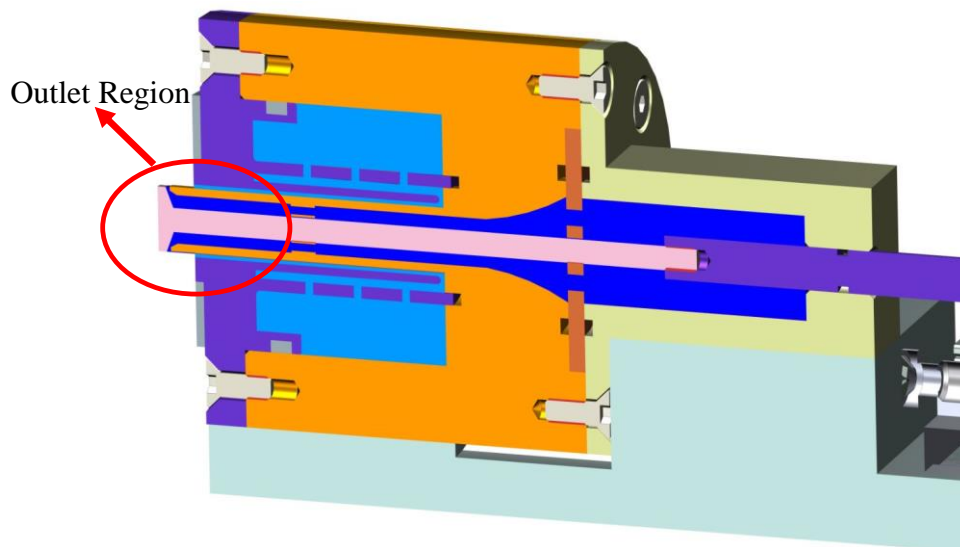


*Figure 2.7 A Cross Section of Movable Mechanism*

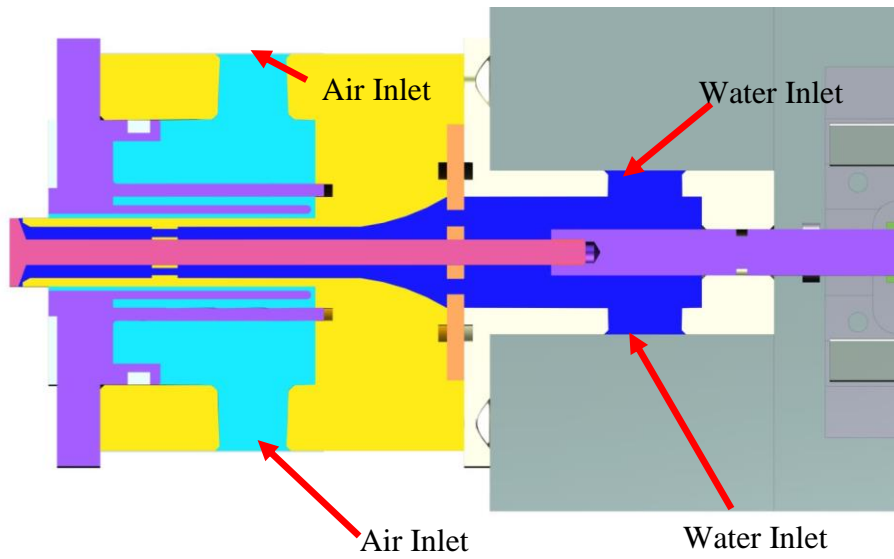


*Figure 2.8. Cross Section of Moveable Mechanism from Top*

In addition to the oxidizer inner geometry, fuel inner geometry is also revised and a 72 hole flow stabilizer is designed for uniform flow (Figure 2.7 and Figure 2.8). This design is carried according to Bedard et al's study [7] and the number of holes and the dimensions are chosen indiscriminately. This design is chosen as the final design to be tested by PDPA system and shadowgraph technique because more stabilized flow and pintle mounting are observed in this design.

## CHAPTER 3

### EXPERIMENTAL SETUP AND RESULTS

#### 3.1. Introduction

The pintle injector's flow physics is a lot more different than the conventional injector types and several studies are still being conducted on this injector type. A few numerical studies carried to explain the flow dynamics of pintle injector. Experimental researches are conducted to investigate the spray characteristics in several different countries. For further investigation of the spray characteristics, a set of experiments are performed at TÜBİTAK SAGE cold-flow experimental facility on behalf of this study. In this chapter, experimental equipment used is introduced firstly. After that, experimental setup and methodology are explained. Finally results of the experiments are given.

#### 3.2. Experimental Equipment

##### 3.2.1. Droplet Generator

A droplet generator is an instrument which produces droplets of uniform size at a certain frequency. It is used for validating droplet particle size measurements. If a reservoir supplying laminar jet is exited periodically at the resonant frequency, the jet transforms into uniform droplets. For this study MDG-100 Monosize Droplet Generator is used. This device has the capability to generate droplets having diameters ranging from 50  $\mu\text{m}$  to 300  $\mu\text{m}$ . From a known jet generated by the droplet generator, PDPA system is validated before the experiments.



*Figure 3.1 Droplet Generator System*

### **3.2.2. Phase Doppler Analysis System**

Phase Doppler Anemometry is a technique which is used for measuring the particle size and velocity. On the contrary to the mechanical methods used for velocity measurements, it is nonintrusive, and it has faster response [13]. Although, it has the same operating principle as Laser Doppler Anemometry technique, the size of the particles are also captured with this technique. The measurement principles are discussed while introducing the components of the system.

This system contains a lot of sub equipment and it takes time to setup and align the system itself. Alignment procedure should be conducted in short intervals since the optical tools are affected from environmental factors. The system contains a 5 Watt Ar-Ion Laser, a beam separator which separates laser to green and blue colors, fiber cables supplying laser to transmitter which collides the beams and creates measurement probe, receiver which receives scattered light from measurement probe, a signal processor converting sensor information to electric signals and finally the software processes these signals to find particle size and velocity. The system is outlined in Figure 3.2.

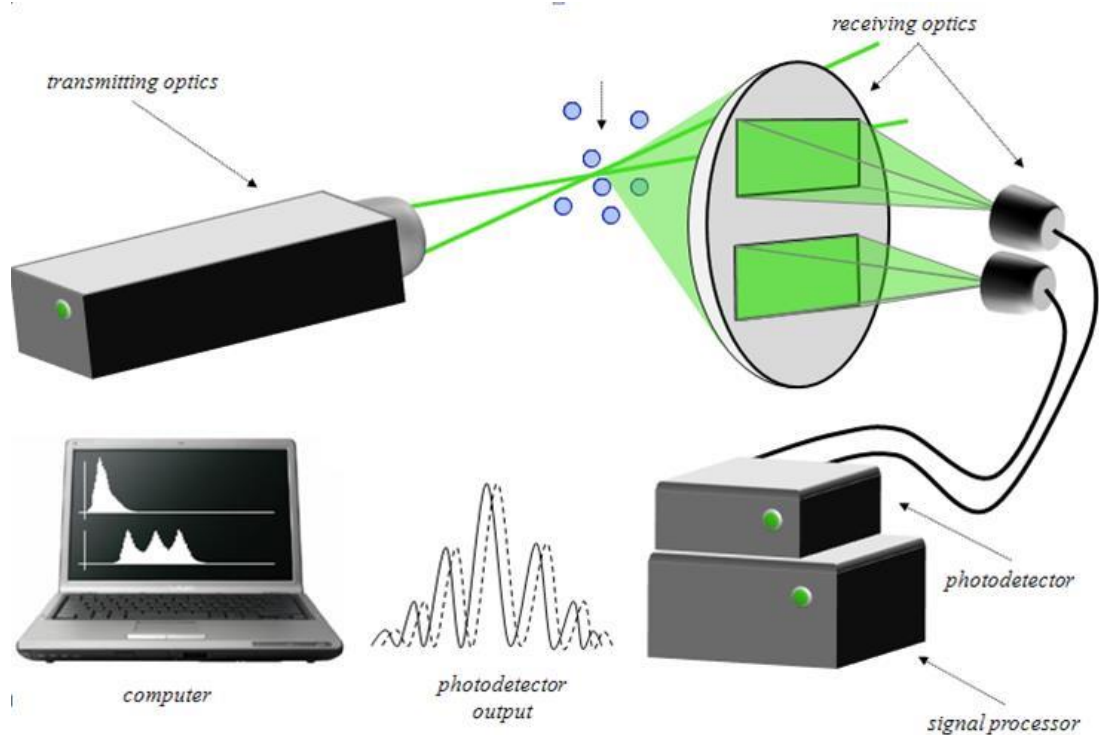


Figure 3.2 PDPA System [15]

First component is Coherent Innova 70-5 Ar-Ion laser which has 5 Watt output. Laser beam is directed to the Fiberlight which is used to divide laser beam into two colors, green and blue. This beam generator consists of a prism and mirrors in which dispersion prism is used to separate green ( $\lambda = 514.5\text{nm}$ ), blue ( $\lambda = 488\text{nm}$ ) and magenta ( $\lambda = 457.9\text{nm}$ ) colors. Furthermore, colors are separated into two beams with different frequencies to create shifted and unshifted beams. These are reflected to the couplers via mirrors. Couplers are used for aligning the focus of separated beams to the fiber optic cables. Laser light is supplied to the transmitter which creates the measurement point.

Transmitter has lenses to collimate beams carried through the cables. It has also a focusing lens which is used for crossing the same colored beams (shifted and unshifted) at the probe. Beam expander may be used for changing the distance of the probe location from the transmitter.

Receiver collects scattered light to 3 detectors which are used for velocity and particle size measurements. These detectors convert scattered light to electric signal and send this signal to FSA signal processor. Signal processor converts electric signal to phase information and sends it to computer. At the software the size and velocity of the particle is stored.

### **3.2.3. Photodiode Power Sensor**

Before every experiment, it is important that both unshifted and shifted laser beams should be at the same power level in order to have correct measurements. Thus, Standard Photodiode Power Sensor (C-Series) from Thor Labs is used to measure the power of lasers which has a range of 50nW to 500mW power and 200 to 1800 nm wavelength covering the green and blue laser's scale of the setup. Laser adjustments are sensitive to environmental factors and laser power may decrease sometimes. This device is used before all experiments to set the maximum power of the lasers.

### **3.2.4. Linear Actuator**

To visualize the transient phenomenon and to be more precise about the pintle opening distance, MTS50/M-Z8 model, a linear actuator is used MTS50/M-Z8 model. The pintle opening distance is closed and at this point linear actuator is set to zero. The encoder inside the actuator provides 29 nm resolution at the given position.



*Figure 3.3 Linear Actuator*

### 3.2.5. High Speed Camera

Atomization process is a highly transient phenomenon. Cone angle oscillates in a high frequency and a high-speed camera is used to measure the correct spray cone angle. FASTCAM SA-Z model high speed camera is used for the experiments which has up to 21000 frames per second (fps) frame rates with megapixel resolution at this fps. The spray is recorded at 5000 frames per second and the images are processed with a MATLAB code to measure the angle. This post processing will be discussed later.

### 3.2.6. Traverse System

PDPA system is used for pointwise measurements and this is the system on which the receiver and transmitter are mounted. Traverse system operates transmitter and receiver at the same time to the predetermined position. Receiver and transmitter can be mounted on it at a desired angle depending on the experiment's scope.

### 3.2.7. Pintle Injector

6 different pintle injectors are designed and tested. In this section the details of each injector are given. Main body of the injectors is kept the same for easy usage. As a result pintle gap thickness, which is the gap surrounding the pintle is the same for every injector type. Pintle tip diameter, shadow angle, tip thickness are the same for every injector. Base geometry of the every injector chosen as it is given in Figure 2.1. The details of the injectors are given in Table 3.1.

Table 3.1. Injector Parameters for Each Type

Injector Type	Pintle Angle	Annular Gap Thickness [mm]	Pintle Tip Diameter [mm]	Pintle Gap Thickness [mm]	Pintle Rod Diameter [mm]
Type-1	20	0.5	8	1.5	3
Type-2	30	0.5	8	1.5	3
Type-3	40	0.5	8	1.5	3

Type-4	20	1	8	1.5	3
Type-5	30	1	8	1.5	3
Type-6	40	1	8	1.5	3

### 3.3. Experimental Methodology

#### 3.3.1. Shadowgraphy with High Speed Camera

Shadowgraph is a proven and simple method used for liquid visualization for almost 2 centuries[14]. The technique uses scattered light from the object being investigated which is captured by a camera. Main concept of the technique is to capture high contrast at the image to investigate the boundaries. The technique has two different methods, the first one is forward scattering where the object is in between the camera and light source as shown in Figure 3.4. The other one is backward scattering where the camera and the light source is at the same side and reflected light from the spray is captured from camera, shown in Figure 3.5. For this study forward scattering is used.

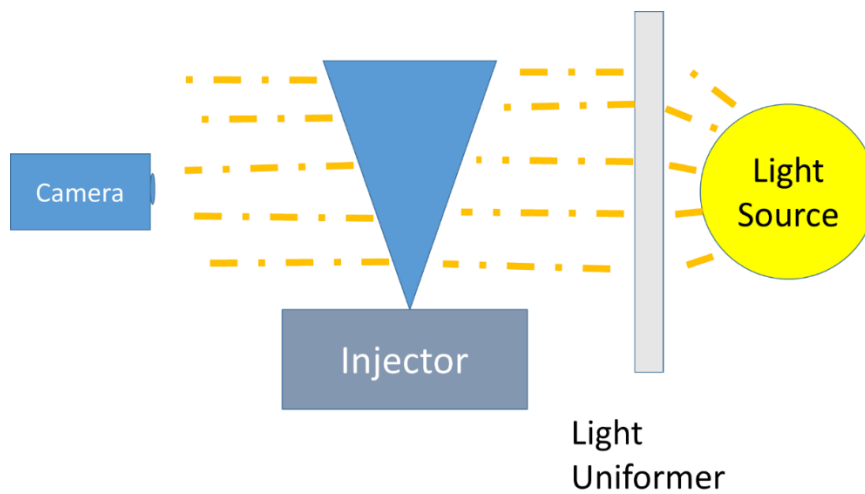
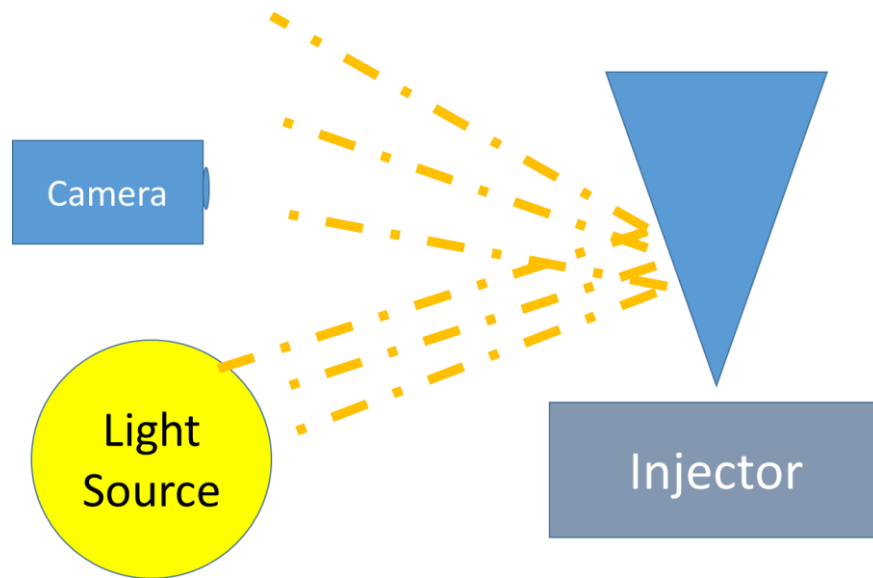


Figure 3.4 Forward Scattering



*Figure 3.5 Backward Scattering*

High speed camera captures 1000 frames per second in a parallel position with respect to spray cone. A white background is fit to obtain a higher contrast. The captured videos are converted to images to be processed by a MATLAB code. Code simply converts RGB images into gray scale to visualize the spray cone. In this way, dense regions become more clear and darker. This image processing process is followed by scaling pixels to millimeters. A benchmark value, which is tip diameter of the pintle, is given as input to the code. This code converts the remaining part of the image to the millimeters and calculates the angle formed by the spray by using the slope of the boundary. Each image is calculated in this way and the average angle is chosen to be the angle of the performed test.

### **3.3.2. Phase Doppler Particle Anemometry**

Particle Doppler Anemometer technique is used for both velocity and diameter size measurements of the particles. Generated laser beams are separated through the components discussed in Section 3.2.2 and at the transmitter the beams are oriented to obtain measurement probe which is also called crossing volume. Since each color has a shifted and an unshifted beam, which have different frequencies, it is obtained a sequential pattern of dark and light fringes at the measurement probe (Figure 3.6).

Thus, as the particle passing through the measurement probe, it scatters light at the light fringes and vice versa occurs for the dark fringes. The receiver receives the scattered light from the particle at a frequency created by the particle. This frequency is proportional to the particle velocity and is known as Doppler shift frequency.

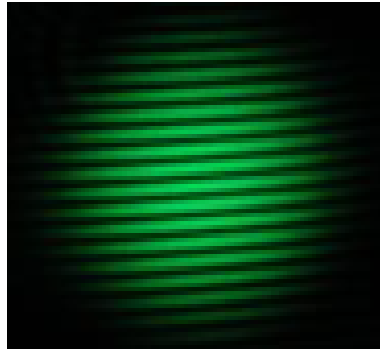


*Figure 3.6 Sequential Pattern of Dark and Light Fringes at Crossing Volume*

In addition to velocity measurements, PDA technique is used for diameter measurements of the particles. Three sensors at the receiver which are located near each other measures the velocity of the particles individually. The light scattered to each spatial location of sensors have different angles and because of this there occurs a phase shift between each sensor. The representation is shown in Figure 3.7 in which sensors are called detector A,B and C. As it can be observed from this figure, two diameter measurements are carried out by the system which are due to the phase shift between sensor A-B and sensor B-C. This makes the technique more reliable and comparable in itself.

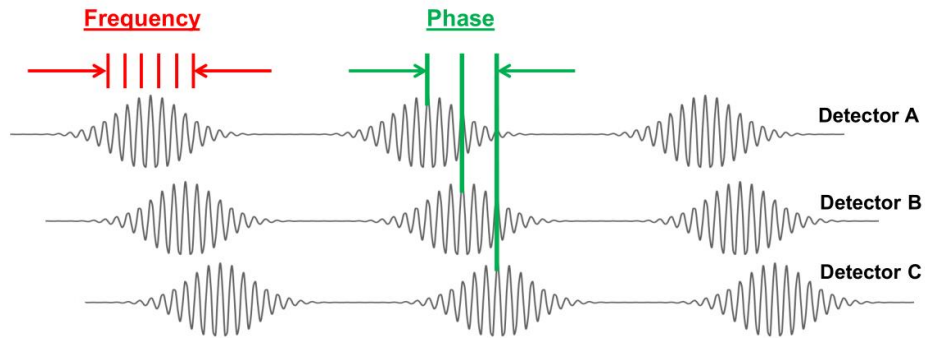


Figure 3.7 . Phase Shift Representation

For this study, 2 component PDPA system is used which means 2 colors are used for velocity measurements. Two colors, green and blue, give ability to measure axial and radial velocities at the same time and forward scatter refraction with 37 degrees is used.

### 3.4. Experimental Setup and Tests

#### 3.4.1. Experimental Setup

In this section, two different test configurations are presented. First experimental setup is the setup for velocity and particle diameter measurement using the PDPA system. The second setup consists of Fast camera instead of PDPA system.

A 10 m<sup>3</sup> air tank supplies air through elastic pipes to a regulator which is set to desired pressure for the test. If the pressure of the air tank is below 9 bar, an automatic compressor starts to increase pressure of the tank. After the regulator, a flowmeter measures the volumetric flow rate of air as a feedback to ensure constant velocity during the test which may take several hours. An orifice is placed just after the flowmeter to obtain choked flow. The orifice size changes from test to test and the information about the orifice is presented at the ‘Tests’ section. It should also be noted that the orifice size is always smaller than the annular part of the pintle, so the choking of the flow is ensured. Following the orifice, the air is supplied to the pintle with the elastic pipes.

Water is stored in a 2 m<sup>3</sup> tank which provides uninterrupted test which may last up to 8 hours. A centrifugal pump supplies water from the tank to the system and a valve is used to control the mass flow rate. A flow meter and a pressure sensor are placed just before the injector to visualize the mass flow rate and the pressure drop through the injector, respectively. There also exist water filters before the flow meter to prevent undesired small particles which could affect the flow especially at orifices.

A data collection system is used to record data during the experiment. Pressure and volumetric flowrates of air and water are collected to check experiment history.

For the first experimental setup PDPA system is placed at the end of the pintle and velocity and size measurements are done. For the second system a light source and the fast camera is placed to do shadowgraphy tests.

### **3.4.2. Experimental Matrix**

6 different injectors which are designed to maximum thrust of 750 N are investigated at 3 different throttle levels. While choosing the cold flow test flow rates for air and water to estimate the design performance, the nondimensional parameter ( $K_3$ ) developed by Son et al [15] is used. The reason for using this parameter is that they have experience with two different experimental setup for both water/air couple and LN<sub>2</sub>/ GN<sub>2</sub> couple. For water/air couple they have performed experiments at atmospheric conditions similar to the experiments performed in this study. On the other hand, cryogenic spray couple LN<sub>2</sub>/ GN<sub>2</sub> is tested in a pressurized tank. They developed  $K_3$  from the combination of these experiments in order to express SMD and spray cone angles in empirical formulations.  $K_3$  is introduced by Eq. (3) in Section 1.1.1 and it includes the effects of the density of simulant fluids and cryogenic fluids

The nondimensional parameter  $K_3$  is calculated for the design condition by Eq. (3) . If  $K_3$  for cold flow experiments is calculated with the velocities at design condition, a different value from the design condition is obtained Thus, there occurs a ratio

between design condition's and cold flow experiment's  $K_3$  value, which is presented in Table 3.2. To make  $K_{dc}$  (geometric parameter for design condition) and  $K_{cold}$  (geometric parameter for cold flow experiment) be equal, basically velocities are changed according to this ratio. Air velocity is always taken as twice of the  $GCH_4$  velocity and water velocity is changed accordingly to satisfy the ratio. The ratio between air and  $GCH_4$  velocity is kept constant because of the limitations of the cold flow experimental setup limitations. Lower velocities for air causes wider sprays which is harmful for PDPA system. The sample calculation for design condition and cold flow experiments are introduced in Table 3.3 and Table 3.4. The mass flow rate of air is the same for all injector experiments since the design condition for methane mass flow rate is constant for all designs and the cold flow transition process is just multiplication of the gas velocity by 2 to satisfy ratio. If one follows the Equation (3) for both design condition and cold flow experiments, he/she can easily notice that the mass flow rates of the water are the same for all injector types which makes it easier to compare.

Table 3.2 Geometric Parameter Calculation For OF=2 Case for Design Condition and Cold Flow Experiment

Injector Type	Velocity GCH4/Air [m/s]	Velocity LOX/Water [m/s]	$K_{dc}$	$K_{cold}$	Ratio
Type-1	167.37/334.75	37.40/16.64	66.41	14.78	4.49

Table 3.3 Geometric Parameter Calculation For 3 different Throttle Levels for Injector Type-1

Throttle Level	Mass Flow Rate of Air [kg/s]	Mass Flow Rate of Water [kg/s]	Mass Flow Rate of $GCH_4$ [kg/s]	Mass Flow Rate of LOX [kg/s]	$L_{tod}$ [mm]	$K_3$
1	0.0049	0.0442	0.0570	0.1140	0.151	66.41
2	0.0036	0.0569	0.0570	0.1140	0.310	37.69
3	0.0030	0.0696	0.0570	0.1140	0.500	25.66

Table 3.4 Geometric Parameter Calculation For 3 different Throttle Levels for Injector Type-4

Throttle Level	Mass Flow Rate of Air [kg/s]	Mass Flow Rate of Water [kg/s]	Mass Flow Rate of GCH <sub>4</sub> [kg/s]	Mass Flow Rate of LOX [kg/s]	L <sub>tot</sub> [mm]	K
1	0.0049	0.0442	0.0570	0.1140	0.151	62.21
2	0.0036	0.0569	0.0570	0.1140	0.310	34.99
3	0.0030	0.0696	0.0570	0.1140	0.500	23.58

In the scope of this study, 18 experiments with 6 different injectors at 3 different throttle levels are conducted. From design condition including the calculations for LOX and gaseous methane to cold flow experiment transition is explained above. Here, the test matrix is given including total momentum ratio, Reynolds number and Weber number for each experiment in Table 3.5. While calculating nondimensional Weber and Reynolds numbers, previous studies are taken into consideration to use the same notation. The equations for Reynolds and Weber are given as follows [5]

$$We = \frac{\rho_{air} L_{open} (V_{air} - V_{water})^2}{\sigma_{liq}} \quad (11)$$

$$Re_{air} = \frac{\rho_{air} V_{air} t_{ann}}{\mu_{air}} \quad (12)$$

$$Re_{water} = \frac{\rho_{water} V_{water} L_{open}}{\mu_{water}} \quad (13)$$

Table 3.5 Experimental Matrix for 6 Injector

Injector Type	Experiment Number	O/F Ratio Simulated	Mass Flow Rate of Air [g/s]	Mass Flow Rate of Water [g/s]	TMR	Reynolds Number Air/Water	Weber Number
Type-1	1	2	2.4	44	1.69	4965/2813	46.48
	2	3	1.8	57	2.49	3724/3676	55.53
	3	4	1.5	69	3.31	3103/4497	63.26
Type-2	4	2	2.4	44	1.66	4965/3061	45.55
	5	3	1.8	57	2.46	3724/4013	54.57
	6	4	1.5	69	3.28	3103/4927	62.23
Type-3	7	2	2.4	44	1.62	4965/3467	44.07
	8	3	1.8	57	2.42	3724/4551	53.06
	9	4	1.5	69	3.24	3103/5599	60.64
Type-4	10	2	4.7	44	0.94	9184/2813	39.02
	11	3	3.5	57	1.41	6839/3676	46.03
	12	4	2.9	69	1.89	5667/4497	51.87
Type-5	13	2	4.7	44	0.94	9184/3061	38.17
	14	3	3.5	57	1.41	6839/4013	45.16
	15	4	2.9	69	1.89	5567/4927	50.94
Type-6	16	2	4.7	44	0.93	9184/3467	36.81
	17	3	3.5	57	1.39	6839/4551	43.79
	18	4	2.9	69	1.88	5667/5599	49.51

Since this study is an experimental study, it is important to check calibration of the instruments used and validate these instruments with other methods in order to obtain reliable data. For this reason, droplet generator, which is described at Section 3.2.1, is used. The process of validation is basically generating droplets with known particle size and measuring these with PDPA system.

It is discussed in Section 3.2.1 that if a laminar jet is disturbed at the resonant frequency, the jet transforms into droplets of uniform size. Equation (14) gives the diameter of the particle,

$$D = \left(\frac{6Q}{\pi f}\right)^{\frac{1}{3}} \quad (14)$$

where  $f$  is the excitation frequency,  $Q$  is the volumetric flow rate and  $D$  is the diameter of the particle.

MDG-100 droplet generator has a frequency generator, drop generator head and a syringe, as shown in Figure 3.8. The water is supplied with syringe pump at a known volumetric flow rate and at the drop generator head, the reservoir is vibrated by the frequency generator to form droplets of known size.

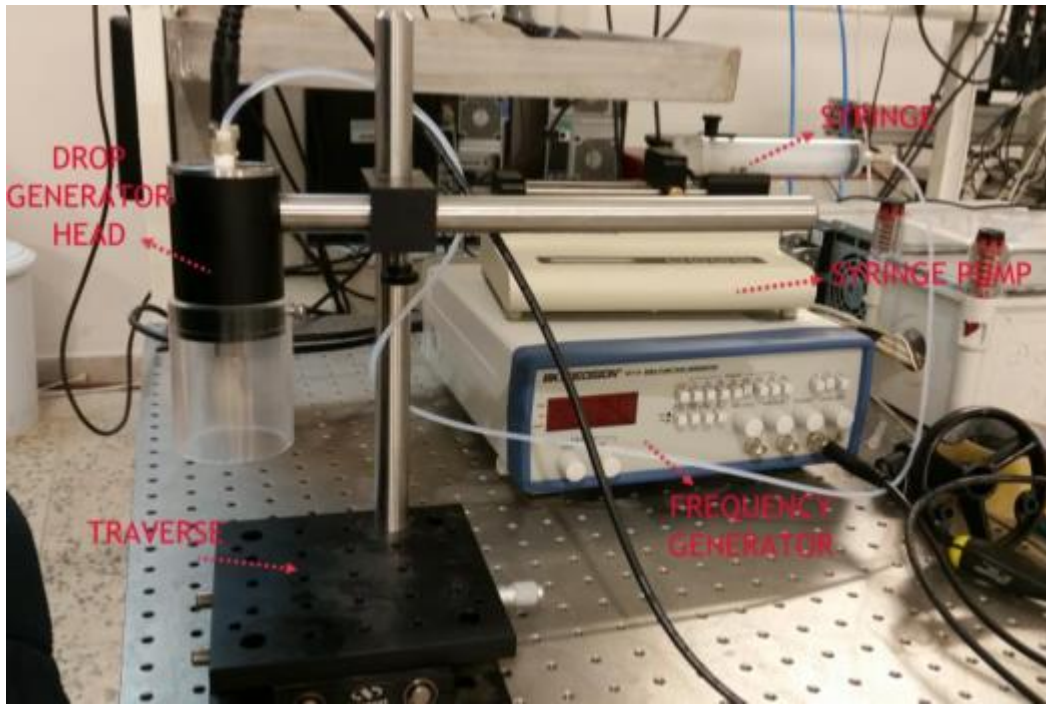


Figure 3.8 MDG-100 Setup

In this study, this process is carried out by 120  $\mu\text{m}$  diameter droplets and PDPA system is used to measure these droplets since this size is the recommended size given by the manual. The measurements and theoretical calculations are presented in Table 3.6. As it can be observed from there, the measurements are carried out with an error of 3% at most which is an acceptable error level for the present work.

Table 3.6 Droplet Generated Droplets Measured by PDPA System

Data Count by PDPA System	Measured $D_{32}$ Size [ $\mu\text{m}$ ]	Theoretical Value Calculated by Equation (14) [ $\mu\text{m}$ ]	Difference Between Calculation and Measurement [%]
49998	116.52	120	2.90
49956	116.73	120	2.73
49921	116.81	120	2.66

### 3.4.2.1. PDPA Experiments' Results

All the experiments are done according to Table 3.5 and in this section Type-1 and Type-4 injectors which have  $20^\circ$  pintle tip angle are considered. 3 different throttle levels are tested for both injectors. During these experiments mass flow rate and pressure drop of water and volumetric flow rate of the air are recorded. For each test spray cone is scanned point by point by the help of the traverse system with 5 mm steps along Y and Z axis (Figure 3.9). ). The measurements start at 1 mm distance from the pintle tip and ends up at 51 mm along x-axis. Only the bottom half of the cone is investigated to maintain the adjustments of the PDPA system during the experiment. Experimental results for Type-1 and Type-4 are presented in this section as they have  $20^\circ$  pintle tip angle and the other type are given with Appendix A. The axial velocity, radial velocity and sauter mean diameter results for experiments (Experiment 1, 2, 3, 10, 11, 12) on injectors Type-1 and Type-4 are given with the following figures. Streamlines are represented using axial velocity values, because of that axial velocity figures are represented by contours both with contours and YZ plots. The YZ plots are given for  $1.25 D_t$ ,  $2.5 D_t$ ,  $3.75 D_t$ ,  $5 D_t$  and  $6.5 D_t$  which corresponds to 10 mm, 20 mm, 30 mm, 40 mm and 50 mm basically for each injector type.

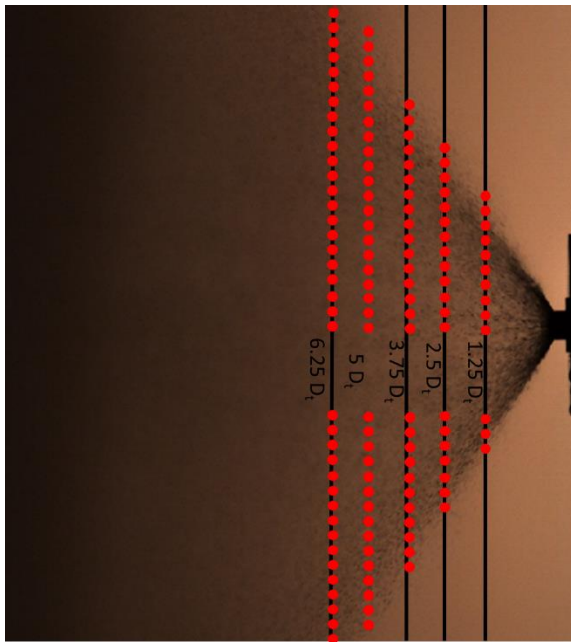


Figure 3.9 Pointwise Measurements on Spray Cone

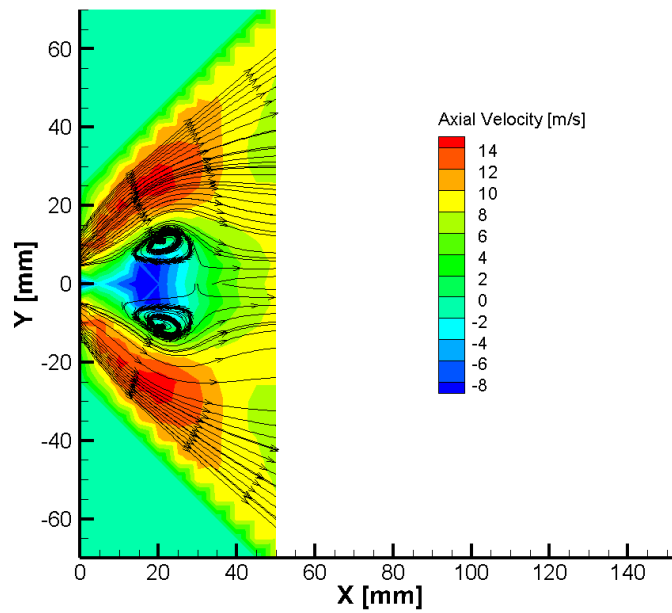


Figure 3.10 Axial Velocity Contour of Experiment 1

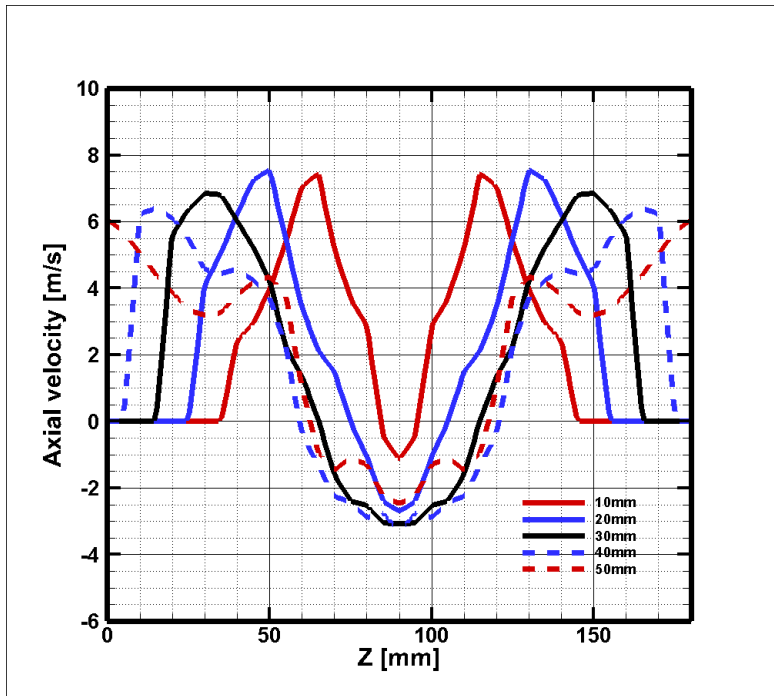


Figure 3.11. Axial Velocity Plot of Experiment 1

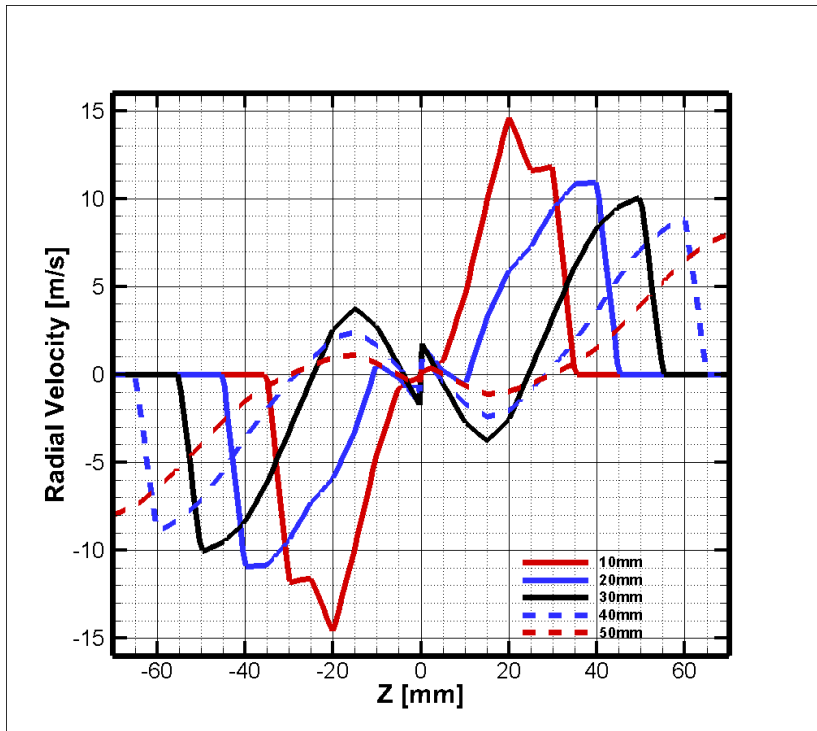


Figure 3.12 Radial Velocity of Experiment 1

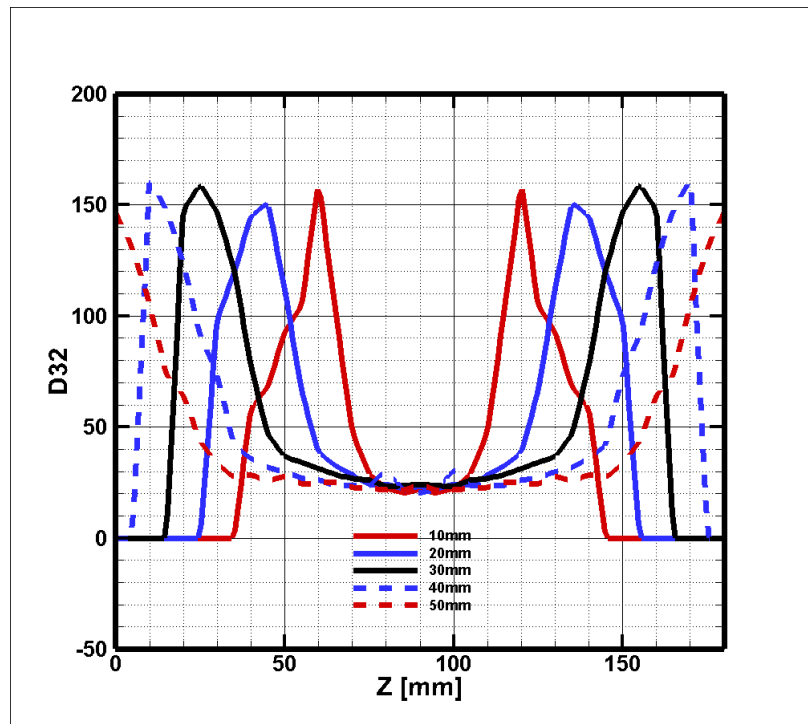


Figure 3.13. Sauter Mean Diameters for Experiment 1

For Experiment 1, two recirculation zones are captured nearly 25 mm away from the pintle tip shown in Figure 3.10 which is a typical pintle injector characteristics. However, the contour is not very smooth since PDPA is a pointwise measurement technique. If the XY plot of the axial velocity is investigated, it can be observed that the velocity decreases towards to the symmetry axis of the pintle. Moreover, one can also observe negative velocity components along X axis which can be visualized better as recirculation zone on the contour plot. If Figure 3.9 is investigated, from  $2.5 D_t$  to  $6.25 D_t$  SMD values are close to  $20\mu\text{m}$ . Other experimental results are given at Appendix-A.

The comparison for axial velocity, radial velocity and SMD values for different O/F ratios in Experiments 1, 2 and 3 are given in Figure 3.14, Figure 3.15, Figure 3.16 and Figure 3.17, respectively.

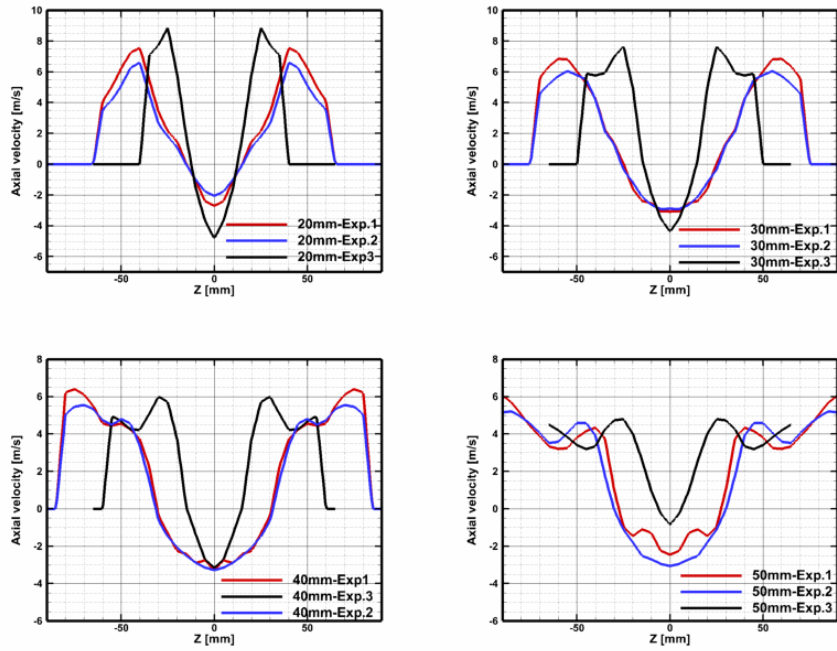


Figure 3.14 Axial Velocity Plots for Experiments 1,2 and 3

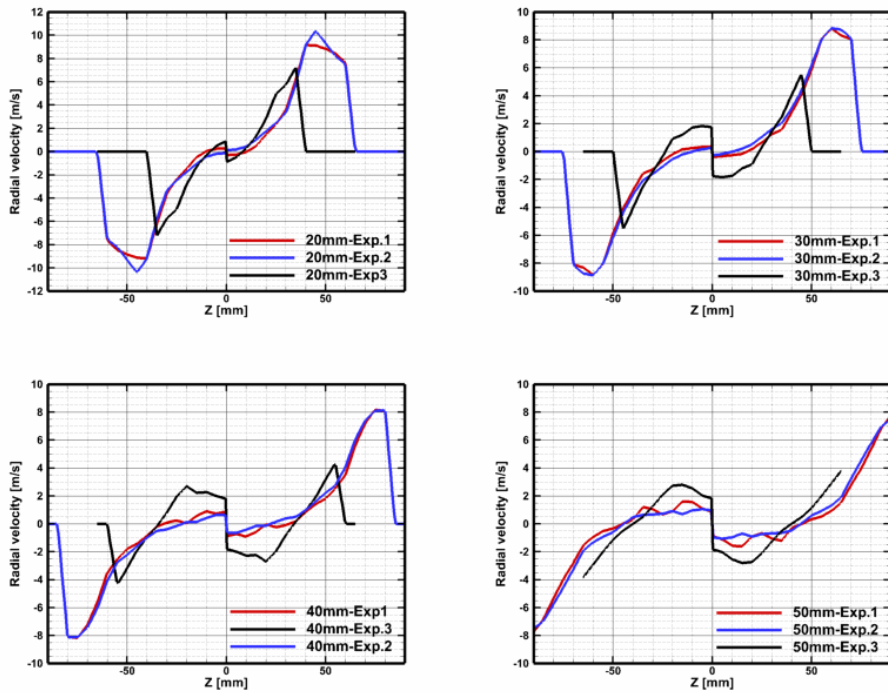


Figure 3.15 Radial Velocity Plots for Experiments 1,2 and 3

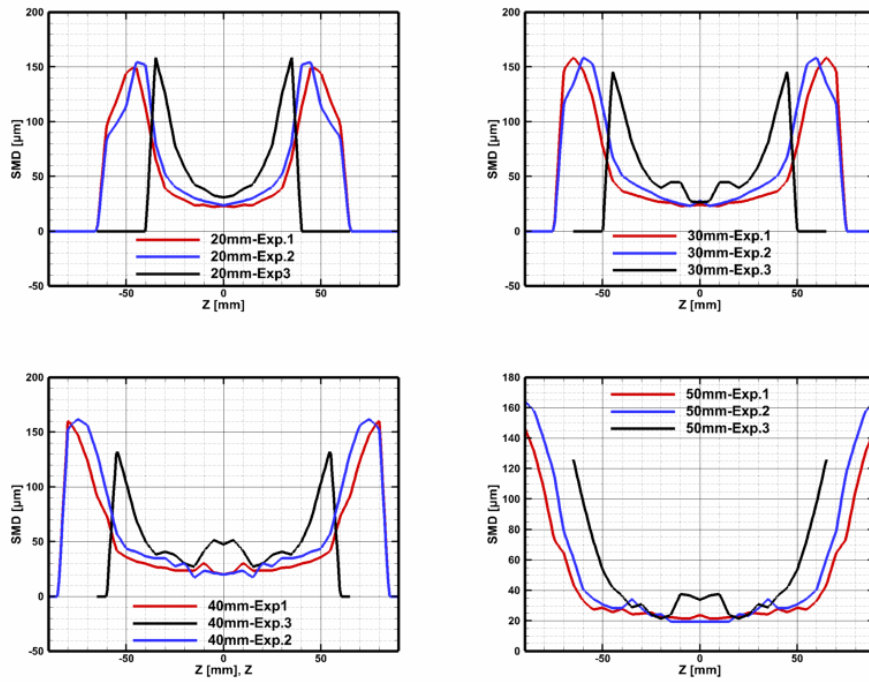


Figure 3.16 SMD Value Plots for Experiment 1,2 and 3

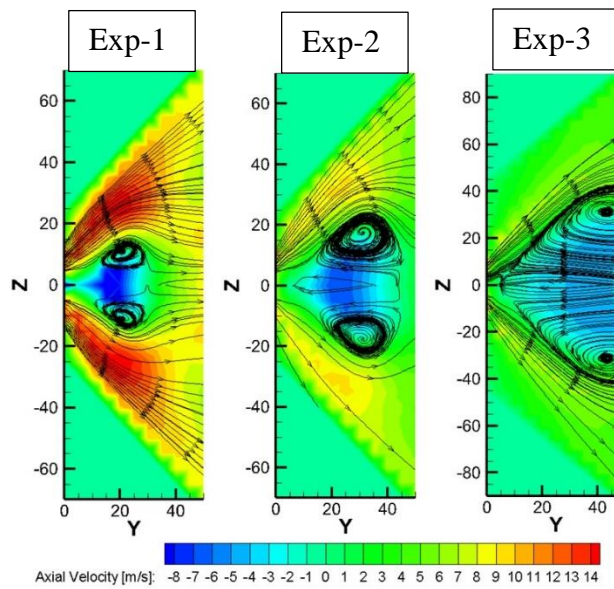


Figure 3.17. Streamlines For Experiment 1,2 and 3

It can be observed that with decreasing characteristic number  $K_3$ , SMD values are getting higher. If Figure 3.16 is investigated, it can be seen that during an experiment (like Experiment 2 at 40 mm) sharp increases may occur. The reason of this increase is the optical alignment and adjustments are kept same during the experiment for all measurement points which leads to have less data to be processed. There is another phenomenon observed that particle size increase at the end of the recirculation zones. Figure 3.17 shows the vortices. As it can be seen from this figure, recirculation zones of experiments 1 and 2 could not be captured entirely. On the contrary, with decreasing  $K_3$ , recirculation zone position gets closer to the pintle tip. This recirculation zone position difference affects the particle size distribution because it is observed that at the far end of the recirculation zones particles are bigger in size. Moreover, particles maintain their size constant relatively along Y-direction after the recirculation zones. To better understand this, Figure 3.16 and Figure 3.20 can be investigated. At 40 and 50 mm for experiment 3 axial velocity increases and recirculation zone is about to be completed and for these regions there is a certain increase on the SMDs (Figure 3.16 and 3.17). In addition to that, if 40mm and 50mm is compared for this experiment, it is seen that 40 mm has larger particles where vortex has ended (Figure 3.16).

To compare the effect of annular gap, Experiment 10, 11 and 12 results for axial/radial velocity and SMD are presented in Figure 3.18, Figure 3.19, Figure 3.20 and Figure 3.21, respectively.

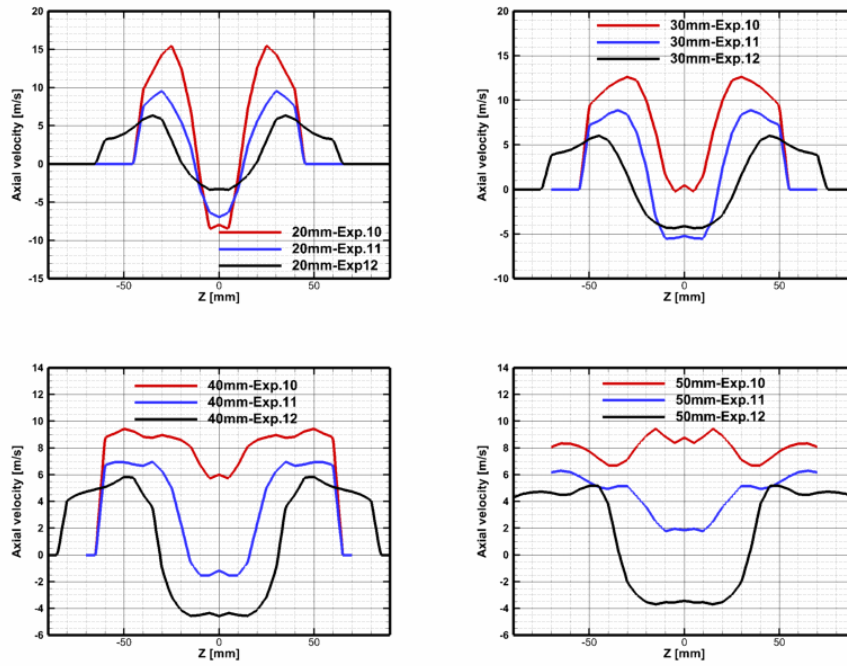


Figure 3.18 Axial Velocity Plots for Experiment 10,11 and 12

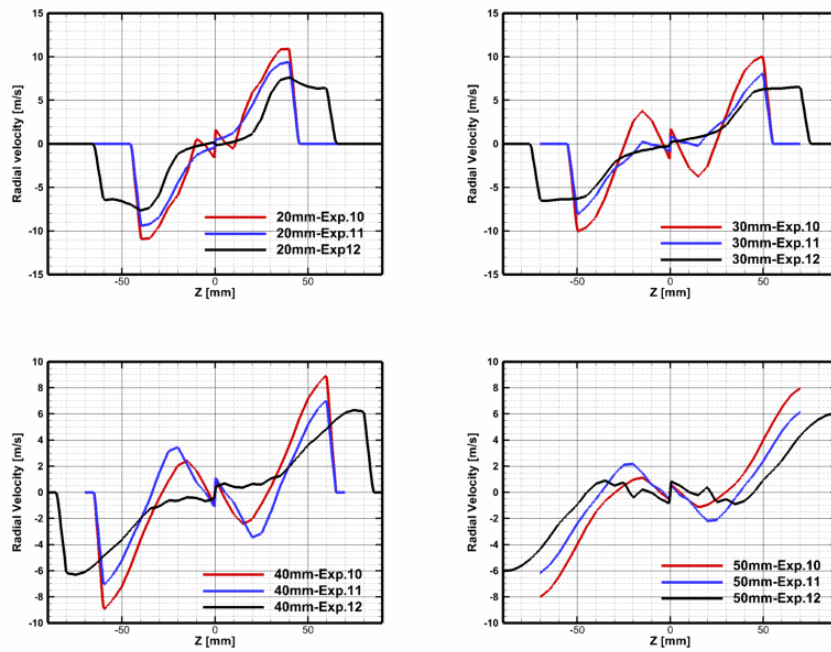


Figure 3.19 Radial Velocity Plots for Experiment 10,11 and 12

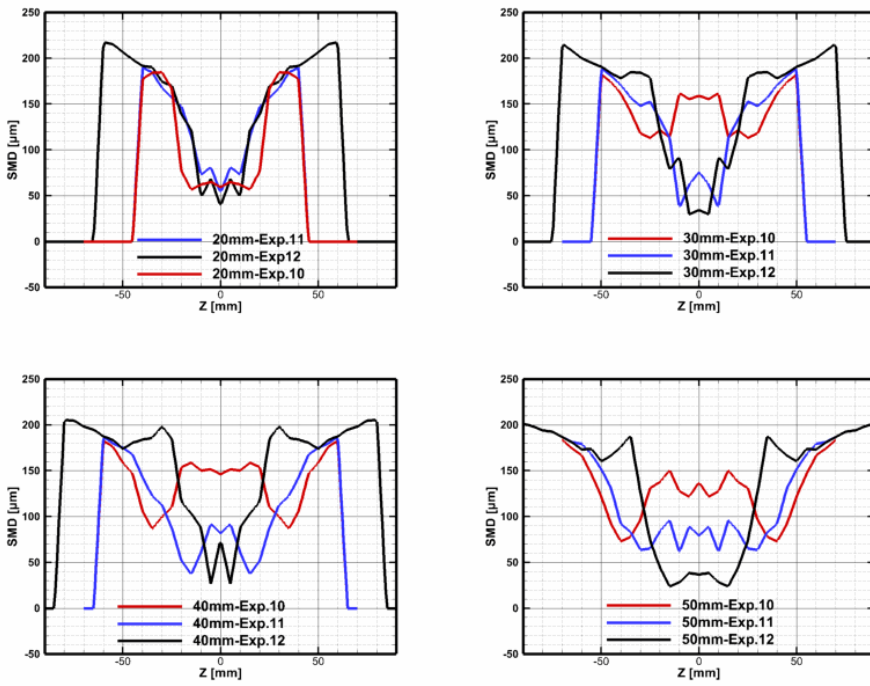


Figure 3.20 SMD Values for Experiments for 10, 11 and 12

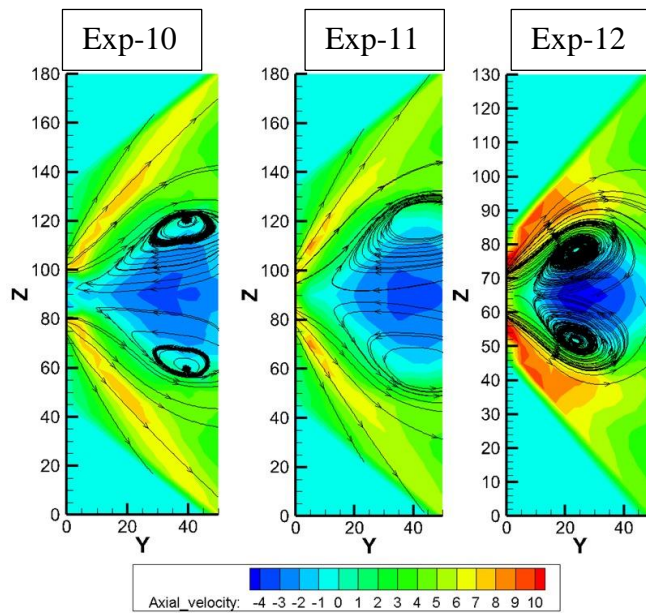


Figure 3.21 Streamtraces for Experiment 10,11 and 12

While increasing the annular gap, air velocity at the annular gap is kept constant which naturally increases the momentum of the air. This situation caused the axial velocities at the liquid sheet to become larger. Moreover, the differences between axial velocities for O/F ratio difference become larger with increasing annular gap. Radial velocities are decreasing more than experiments 1-2-3 bundle along Y axis because the momentum increase as the annular gap increases. For annular gap comparison the biggest difference observed in the SMD values. If Figure 3.16 and Figure 3.20 are compared, one can observe that higher SMD values are obtained for the larger annular gap. In addition to that, recirculation locations extended further to the pintle tip compared with experiment 1,2 and 3 recirculation locations. This phenomenon is thought to be related with decreasing TMR compared with these experiments.

Moreover, to compare the effect of pintle angle Experiment 1,4,7 are given in Figure 3.22, Figure 3.23 and Figure 3.24. Recirculation zones are observed only for 20° pintle angle and for 30° and 40° pintle angles they are not captured. Experiment 1 has a wider spray cone and SMD pattern is more uniform compared with the wider pintle angles. Axial velocities of the droplets increase as the pintle tip angle increases. This increase is correlated with the water momentum and narrow spray cone. Moreover, it is seen that the greater the pintle tip angle, the bigger droplet sizes.

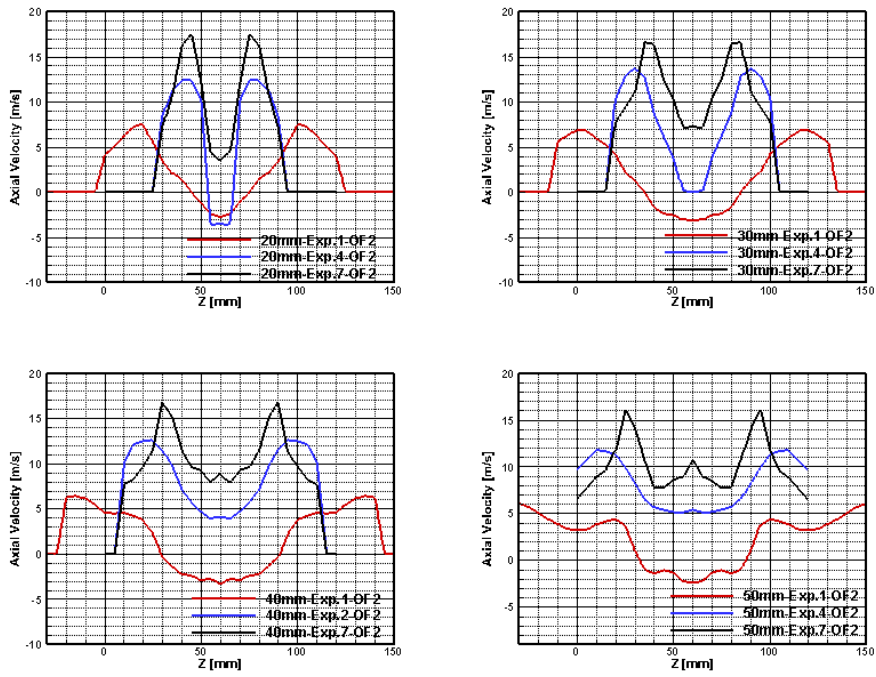


Figure 3.22 Axial Velocities for Experiments 1,4 and 7

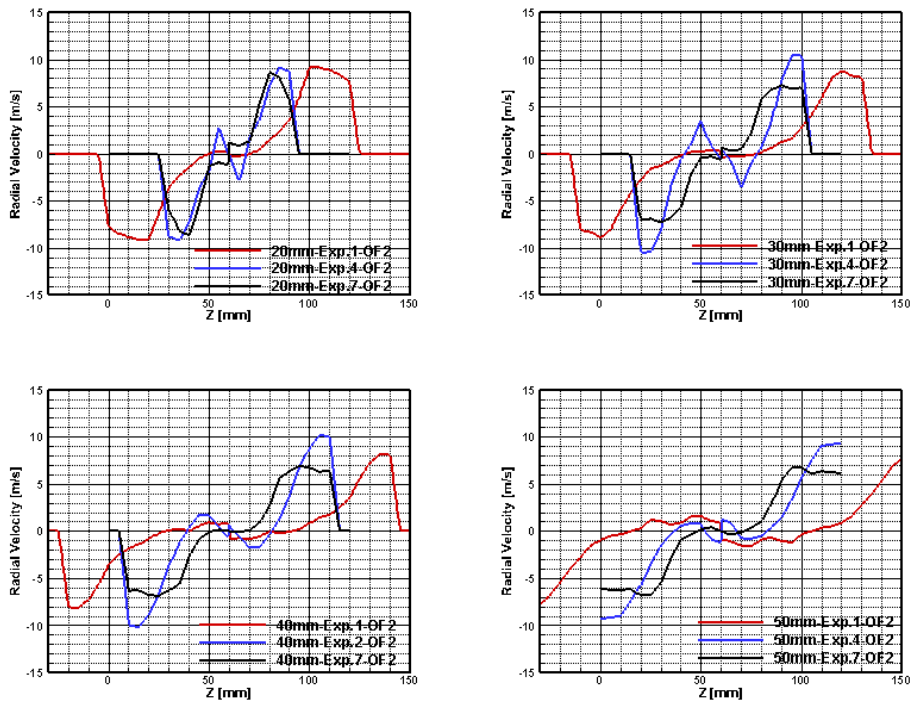


Figure 3.23 Radial Velocities for Experiment 1,4 and 7

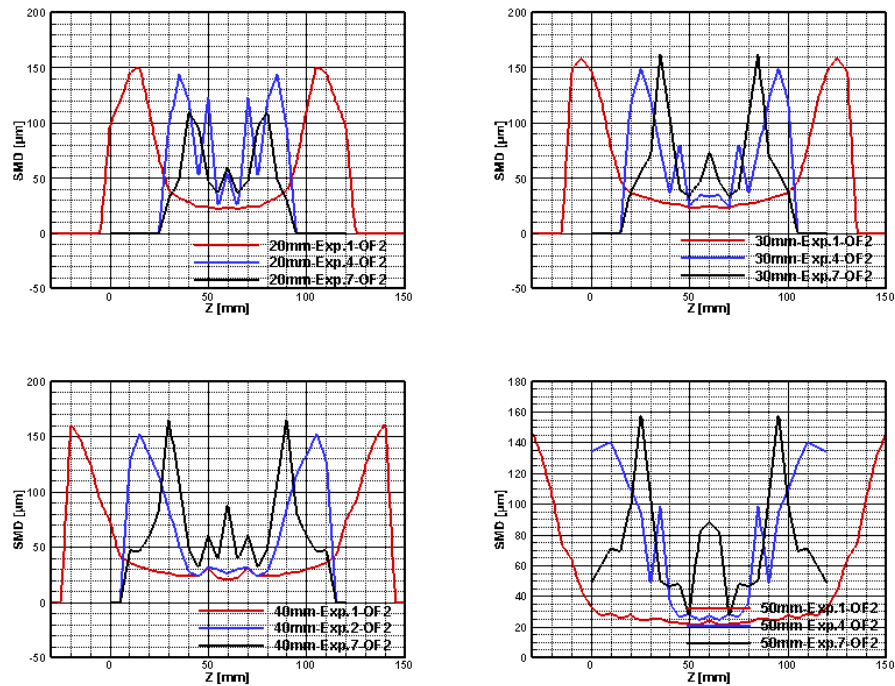
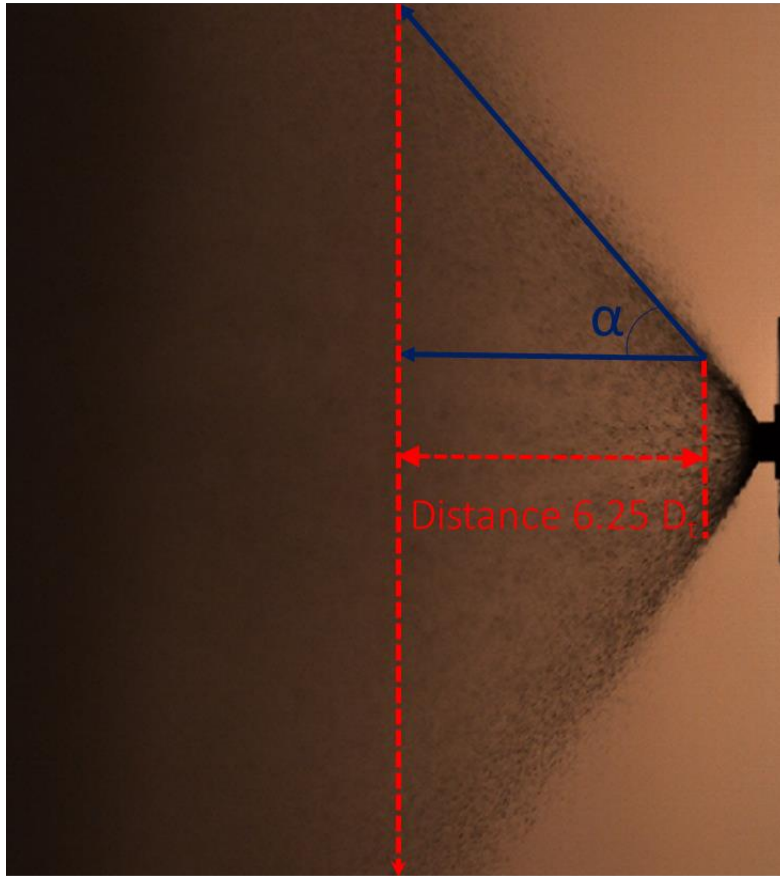


Figure 3.24 SMD Values for Experiments 1,4 and 7

### 3.4.2.2. Shadowgraph Experiments Results

In this section, spray angle measurements are presented and discussed. In addition to given experiment of matrix , 48 experiments are conducted to obtain more information about spray cone formation depending on the flow rates and geometrical parameters. The angle measurement is achieved by a MATLAB code in which two lines are given as inputs. The distance between these lines are  $5D_t$  and the first line is selected near to pintle tip manually (Figure 3.25). Along these lines, the code detects the points where the contrast changes most and it stores the pixel value at these points. This process is applied for each frame along the experiment duration which is at least 20 ms. As discussed before 10000 frames per second is the record rate to eliminate the fluctuations during the experiment. At the end, code calculates the average spray cone angle from all obtained in the experiment.



*Figure 3.25 Spray Cone Angle Measurement with Shadowgraph Technique*

The shadowgraph images from Experiment 1, 2, 3, 10, 11 and 12 are given in Figure 3.26 and Figure 3.27. These two figures show the effect of annular gap, other experimental conditions such as mass flow rates and geometrical parameters are kept constant. Figure 3.26, Figure 3.27 and Figure 3.28 is given for to compare pintle tip angle effect.

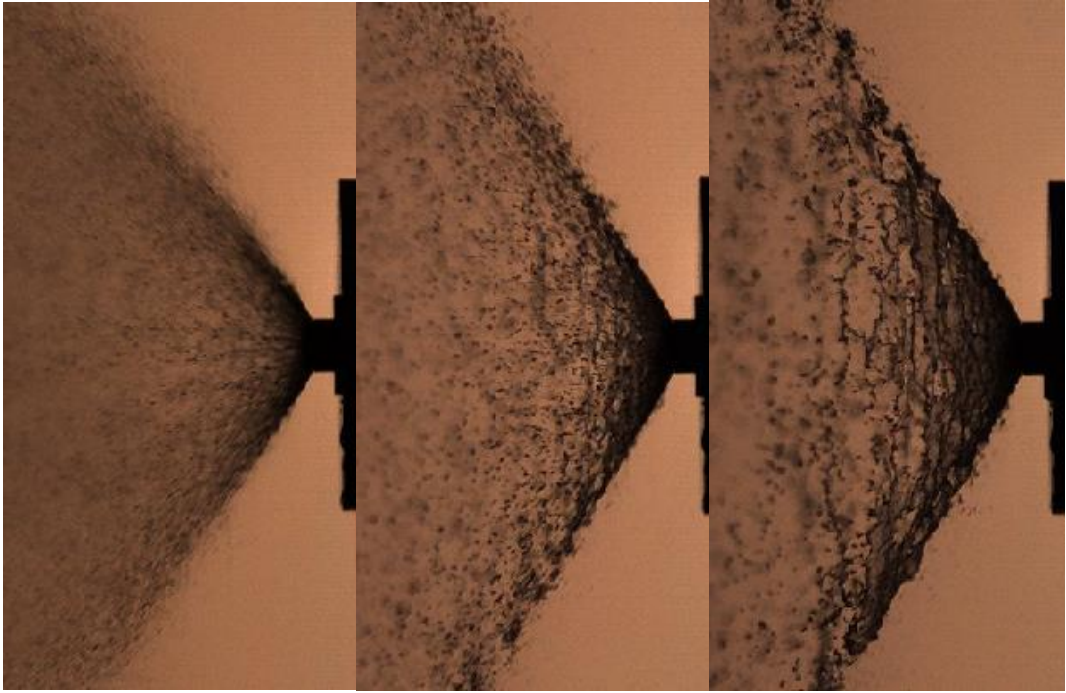


*Figure 3.26 Spray Cone Formation of Experiment 1,2 and 3*

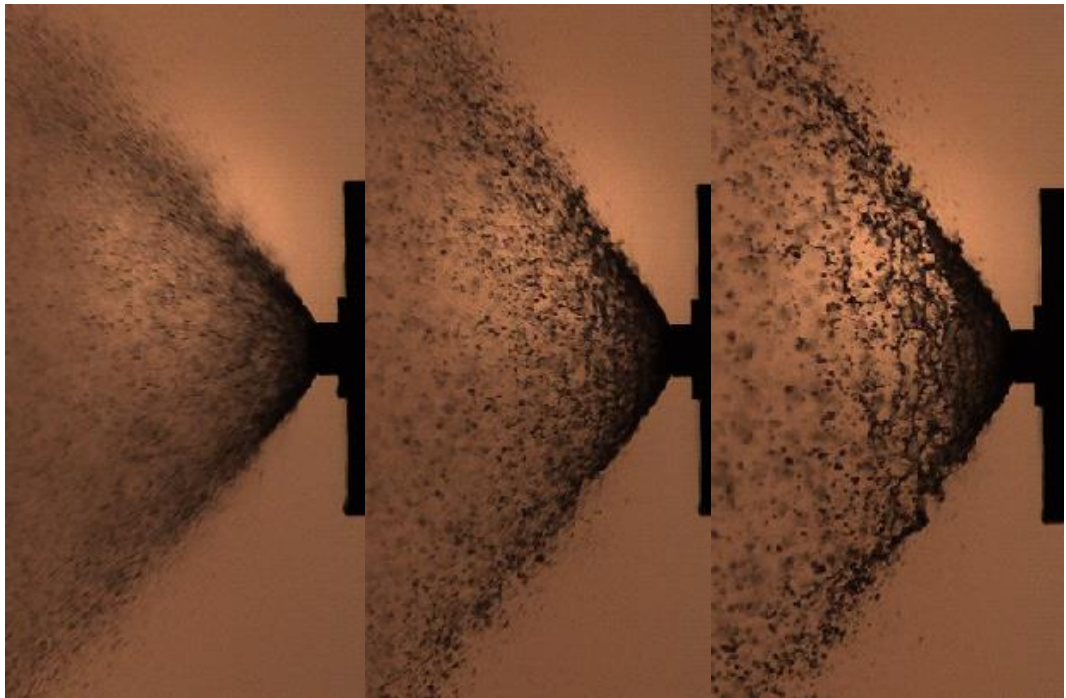


*Figure 3.27 Spray Cone Formation of Experiment 10,11 and 12*

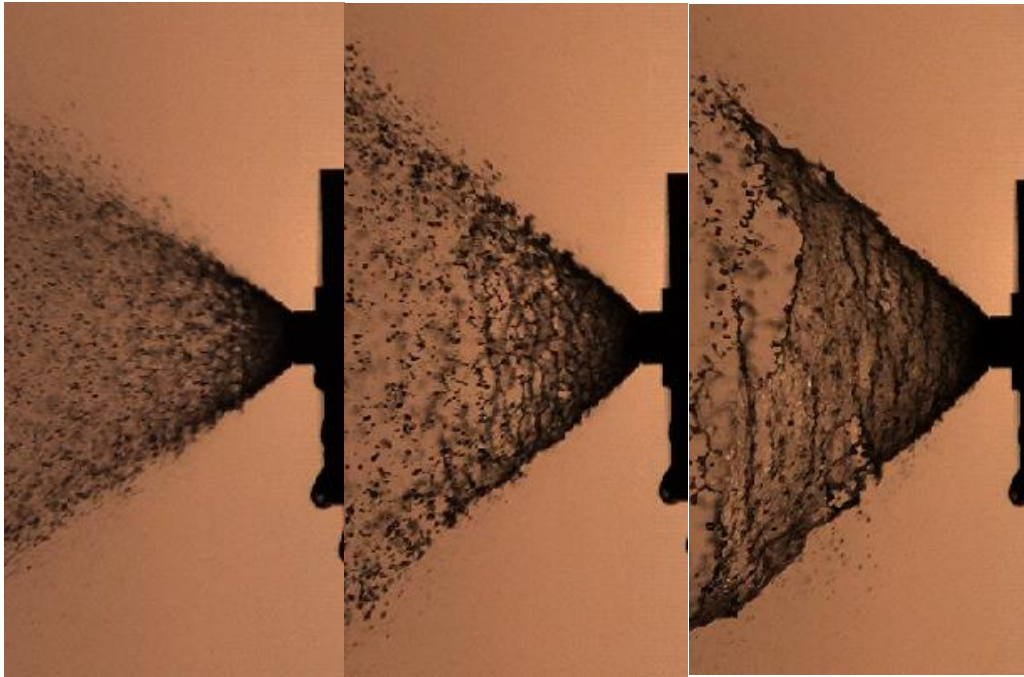


*Figure 3.28 Spray Cone Formation of Experiment 4,5,6*

For Experiment 1,2 and 3 the spray half angles are measured to be  $51.44^\circ$ ,  $57.38^\circ$  and  $57.79^\circ$  respectively (Figure 3.26). When annular gap thickness is increased, the spray half angles become  $50.30^\circ$ ,  $52.21^\circ$  and  $53.44^\circ$ , respectively (Figure 3.27). As expected, an increase in the annular gap contracts the spray half angle observed from the Figure 3.27 and Figure 3.28 since the velocity is kept the same for both annular thicknesses. Moreover, primary breakup is observed to be closer to the pintle tip compared with the thinner annular gap. In addition to these comments, another comparison is performed for the pintle tip angle. The increase in the tip angle makes pintle tip to get contracted and it gets closer to the water flow direction. This makes spray half cone angle to be narrower. It can also be seen that for experiment 6, similar to experiment 3, primary breakup occurs further away from the pintle tip.

As stated, before more experiments are performed and mass flow rates and pintle tracing distances for experiments are presented in Table 3.7. The reason to conduct these experiments is to gain more experience with cold flow test procedure of the

injector designed. Shadowgraph tests are easier and shorter compared with PDPA experiments and to have better understand on the spray cone angle correlations, mass flow rates chosen in Table 3.7 are used in shadowgraph experiments.

*Table 3.7 Experiments Performed Other Than Design Condition Simulation*

Injector Type	Pintle Tracing Distance [mm]	Mass Flow Rate of Water [g/s]	Mass Flow Rate of Air [g/s]
Type-1		83.3	
Type-2	0.322	100.0	4.7
Type-4	0.5	116.7	
Type-6		133.3	
Type-1	0.322	100.0	3.5
	0.5	116.7	
		133.3	
Type-3	0.322	100.0	2.4
	0.5	116.7	
		133.3	

The results for these experiments are expressed in terms of nondimensional parameters for better visualizing. Figure 3.29 gives the characteristic number  $K_3$  (defined by Equation (3)) versus spray angle measured from shadowgraph and Figure 3.30 gives the TMR versus Weber number. As characteristic number is kept constant and pintle angle is decreased, it is observed that spray half cone angle is increasing. Moreover,

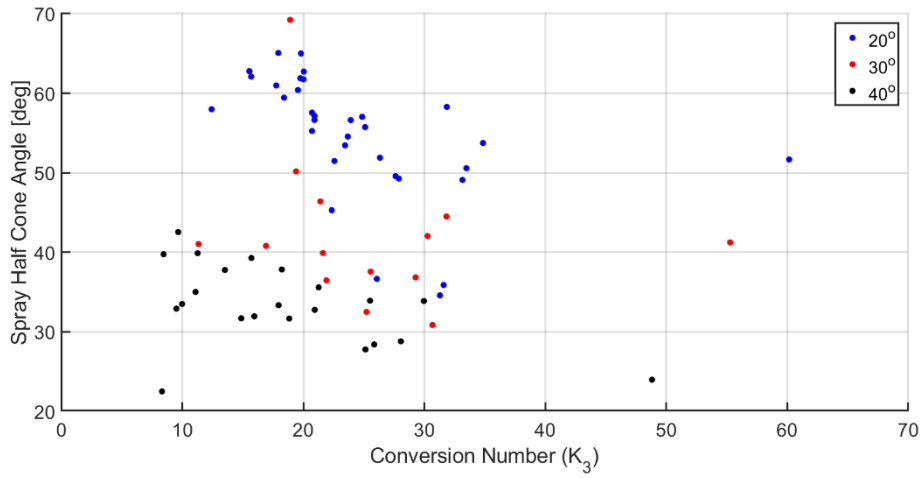


Figure 3.29 Characteristic Number vs Spray Half Cone Angle

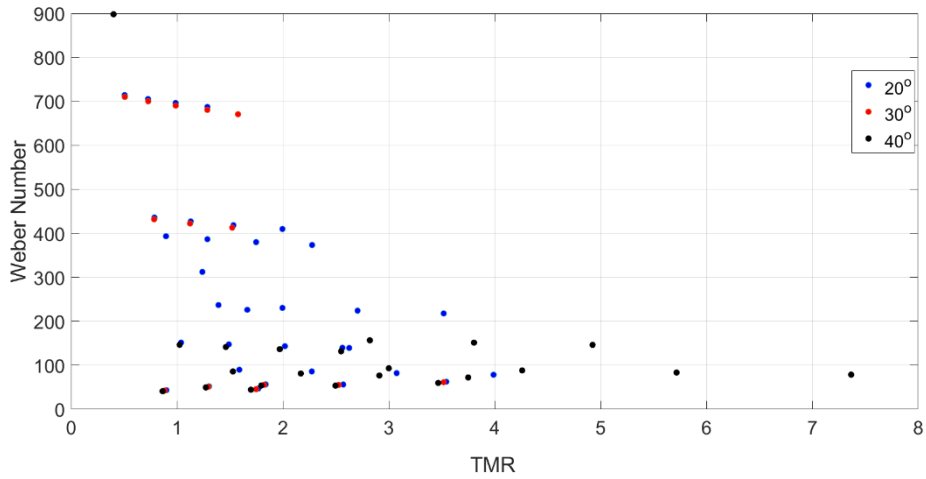


Figure 3.30 TMR versus Weber Number

In their work Lee et al. proposed a new characteristic number defined by Equation (3). As it is stated in that study,  $K$  is the most important parameter to estimate spray half cone angle (Equation (15) and Equation (16)) [5].

$$\theta_{spray} = 90 * \xi * \exp\left(\frac{S - 0.2}{1 + \left(\frac{K}{90}\right)^p} - S\right) \quad (15)$$

$$\xi = \frac{90 - \alpha}{90} , \quad S = 1.15 + 1.35\xi , p = 1.30 + 0.90\xi \quad (16)$$

If this correlation is used the present study, average difference between the estimation and the real values is 14.63 % which is acceptable if the experimental conditions are considered. The estimation and experimental values are given in Figure 3.31.

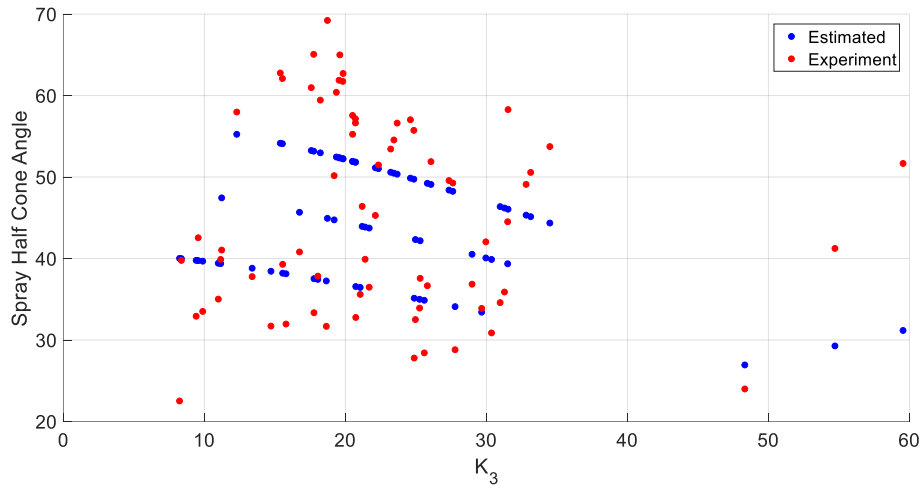


Figure 3.31 Experimental and Estimated Spray Cone Angle Values

Differences here may be caused by different experimental conditions such as significant Weber number difference. Weber numbers for this study are relatively compared to the other studies because of the experimental limitations. Although these differences exist, from the literature the best matched correlation is this one and it is chosen to be used for this study. More detailed images of the shadowgraph test is given in Appendix-A.



## CHAPTER 4

### CONCLUSION

In this study, first the former designs and design methods of pintle injectors are investigated. A design analogy for LOX/GCH<sub>4</sub> liquid rocket engine injector is presented in terms of geometrical and performance constraints. 6 different designs with 3 different pintle angles and 2 different annular gaps are designed in order to be tested. By the help of former studies, non-dimensional parameters are used to represent hot flow design conditions to cold flow experimental matrix. Water and air are used as simulants of the real propellants. Cold flow experiments are conducted at the desired points. All injectors are designed to have 750N thrust at the highest throttle level and throttle ratios up to 3:1.

Reservoir geometry is also investigated. 3 different inner geometries are tried to obtain uniform and axisymmetric spray cone at the outlet of the designs. Each reservoir design is produced and tested mechanically. At the end, for both air and water flow holed structures for inner geometry is decided to sustain uniform flow.

Two component PDPA experiments are carried out to measure axial/radial velocity and Sauter mean diameters of the spray droplets. While converting to the hot flow mass flow rates to the cold flow mass flow rates, a multiplier is used because transmitter and receiver of the system is capable of a limited spray cone. They might get wet which is an undesired condition; thus, multiplier is chosen to have relatively smaller spray cones. According to experiments conducted, for 20° pintle tip recirculation zones occur which is a characteristic of pintle injectors. However, for 30° and 40° no recirculation zones are captured and axial velocities are always on positive direction.

It is observed that Sauter Mean Diameters are increasing at the end of the recirculation zones for 20° pintle tips for both annular gap thicknesses. In addition to that annular

gap thickness increase moves away the existing recirculation zones from the pintle tip which also increases the distance of the particle collision and particle size increase. To have recirculation zones every experiment tried, different indicators can be arranged to have different mass flow rates for future work. To compare 6 designs in SMD size, Type-1 injector has the lowest particle sizes with the lowest pintle angle and annular gap thickness. This is a desired condition for a combustion chamber which provides higher burning area. Type-1 has lowest pintle angle which provides wider spray cone with smaller droplets and in addition to that, it has thinner annular gap thickness which gives better atomization.

Spray cone angle is also investigated by shadowgraph technique to understand geometrical features on the cone. Forward scattering is used to visualize the spray cones and an image processing tool is used to measure the angle. Angles are measured  $6.25 D_t$  distance from the pintle tip and mean value of the frames captured is assumed to be the spray half cone angle. A high-speed camera is used to capture the images with 10000 fps and high contrast is obtained with optical alignments from the camera. As expected, spray half angles decrease with the increasing annular gap thickness. Moreover, breakup lengths are found to be lower for higher annular gap thickness with same air velocity. More experiments are conducted than the given experiment matrix for PDPA experiments, because it is easier to conduct shadowgraph experiments compared with PDPA experiments. Non-dimensional parameters from literature are used to present the experiment results. These parameters are used to predict the spray half cone angle. A new parameter is not developed because it is thought that not enough experiments are conducted. Considering spray cone angle, again Type-1 injector is the best option with widest cone angle among the others. However, this injector may not be suitable for a hot flow test, because it depends on the mission requirements (cooling, chamber diameter etc.).

For the future work, more shadowgraph experiments may be conducted to obtain a new geometrical parameter for gas-liquid slot type injectors. Different flow rates with new characteristic numbers may be carried out to increase the experience on the flow

rate-flow field relation. It is also noted that cold flow tests are easier and cheaper experiments than the hot flow tests. These tests are conducted to predict the predict the atomization qualities of the hot flow tests. That is why, hot flow tests may be conducted to increase the experience with the linkage between hot flow and cold flow tests.



## REFERENCES

- [1] G. Dressler and J. Bauer, “TRW pintle engine heritage and performance characteristics,” 2000.
- [2] G. Elverum, Jr., A. Hoffmann, J. Miller, and R. Rockow, “The descent engine for the lunar module,” in *AIAA 3rd Propulsion Joint Specialist Conference*, 1967, vol. 67, no. 521.
- [3] R. Gilroy and R. Sackheim, “The Lunar Module descent engine - A historical summary,” in *AIAA/ASM E/SAE/ASEE 25th Joint Propulsion Conference*, 1989.
- [4] M. Son, K. Radhakrishnan, J. Koo, O. C. Kwon, and H. D. Kim, “Design Procedure of a Movable Pintle Injector for Liquid Rocket Engines,” in *Journal of Propulsion and Power*, 2016.
- [5] M. Son, K. Radhakrishnan, J. Koo, O. C. Kwon, and H. D. Kim, “Design Procedure of a Movable Pintle Injector for Liquid Rocket Engines,” *J. Propuls. Power*, vol. 33, no. 4, pp. 858–869, 2016.
- [6] M. Son, K. Radhakrishnan, Y. Yoon, and J. Koo, “Numerical study on the combustion characteristics of a fuel-centered pintle injector for methane rocket engines,” *Acta Astronaut.*, vol. 135, pp. 139–149, 2017.
- [7] M. Bedard, T. Feldman, A. Rettenmaier, and W. Anderson, “Student design/build/test of a throttleable LOX-LCH<sub>4</sub> thrust chamber,” in *48th AIAA/ASME/SAE/ASEE Joint Propulsion Conference & Exhibit*, 2012, p. 3883.
- [8] P. Cheng, Q. Li, S. Xu, and Z. Kang, “On the prediction of spray angle of liquid-liquid pintle injectors,” *Acta Astronaut.*, vol. 138, no. May, pp. 145–151, 2017.
- [9] K. Sakaki *et al.*, “Combustion Characteristics of Ethanol/Liquid-Oxygen Rocket-Engine Combustor with Planar Pintle Injector,” *J. Propuls. Power*, vol. 33, no. 2, pp. 514–521, 2016.
- [10] K. Sakaki, M. Choi, S. Nakaya, M. Tsue, and T. Hiraiwa, “Fundamental Combustion Characteristics of Ethanol/Liquid Oxygen Rocket Engine Combustor with Planar Pintle-type Injector,” *Trans. Jpn. Soc. Aeronaut. Space Sci.*, vol. 58, no. 1, pp. 15–22, 2015.
- [11] K. Gavitt, T. Mueller, T. Wang, H. Thom, C. Murphy, and J. Weede, “TRW LCPE 650 Klbf LO<sub>x</sub>/LH<sub>2</sub> Test Results,” in *36th AIAA/ASME/SAE/ASEE Joint Propulsion Conference and Exhibit*, 2000, p. 3853.
- [12] J. Gromski, A. Majamaki, S. Chianese, V. Weinstock, and T. Kim, “Northrop Grumman TR202 LOX/GH<sub>2</sub> Deep Throttling Engine Project Status,” no. July,

pp. 1–11, 2014.

- [13] W. Bachalo and M. Houser, “Development of the phase/Doppler spray analyzer for liquid drop size and velocity characterizations,” in *20th Joint Propulsion Conference*, 1984.
- [14] B. Sümer, “EXPERIMENTAL AND NUMERICAL INVESTIGATION OF PRESSURE SWIRL ATOMIZERS,” Middle East Technical University, 2014.
- [15] K. Lee, D. Shin, M. Son, H. Moon, and J. Koo, “Flow visualization of cryogenic spray from a movable pintle injector,” *J. Vis.*, vol. 22, no. 4, p. 773, 2019.

## APPENDICES

### A. Velocity and SMD Values of Remaining Experiments

In section 3.4.2.1 experiments conducted for 20° pintle tip are given. The remaining results are given in this Appendix with the following figures.

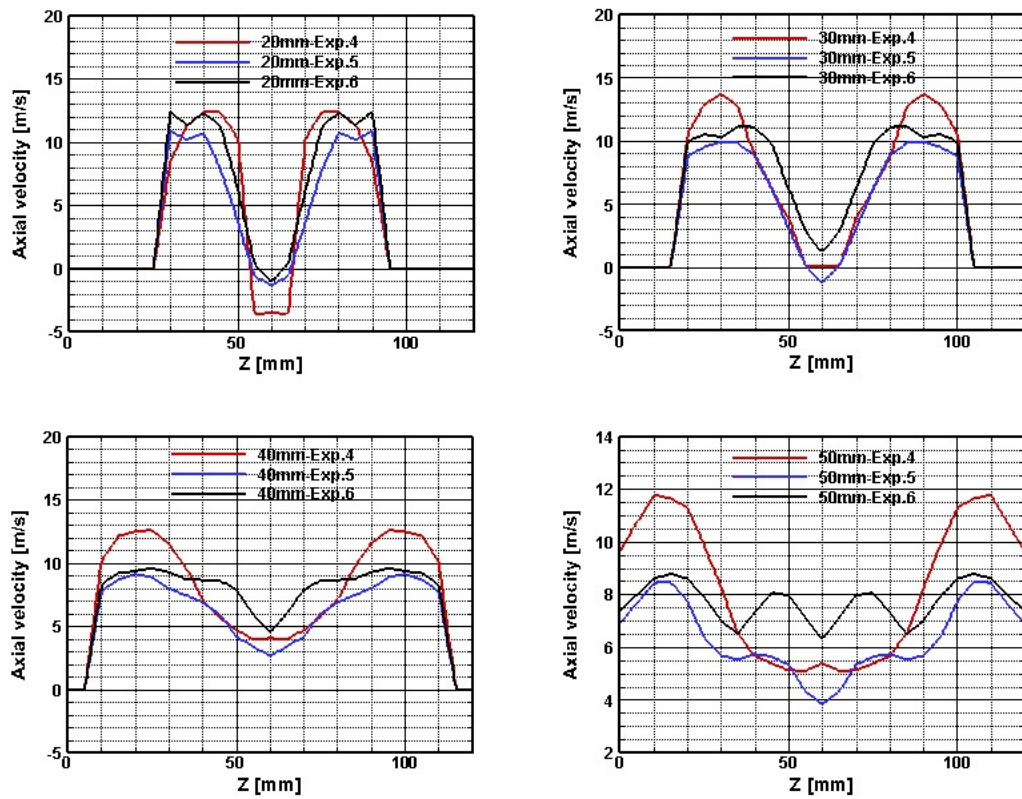


Figure A.1 Axial Velocities for Experiment 4,5 and 6

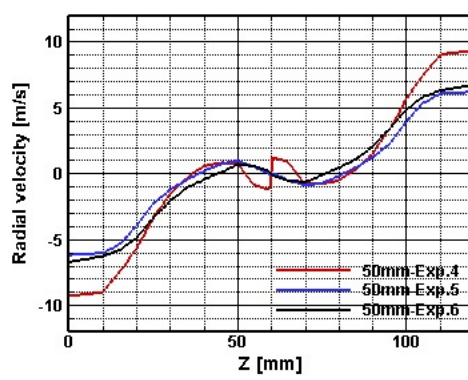
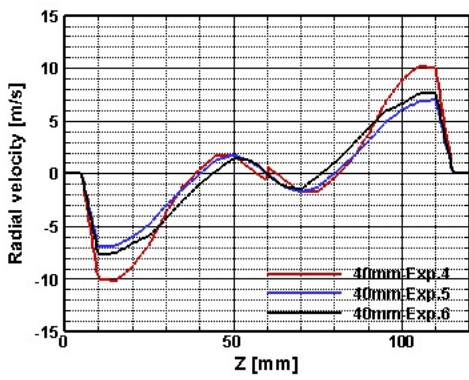
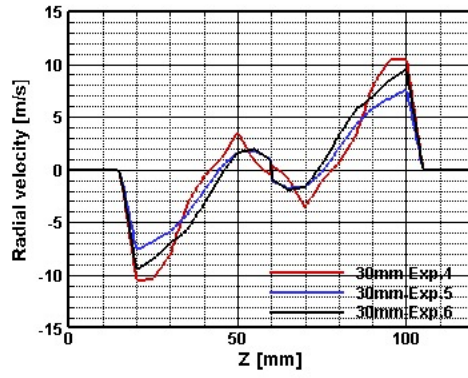
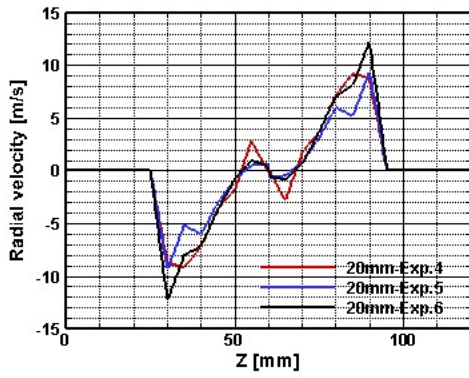


Figure A.2 Radial Velocities Experiments 4, 5 and 6

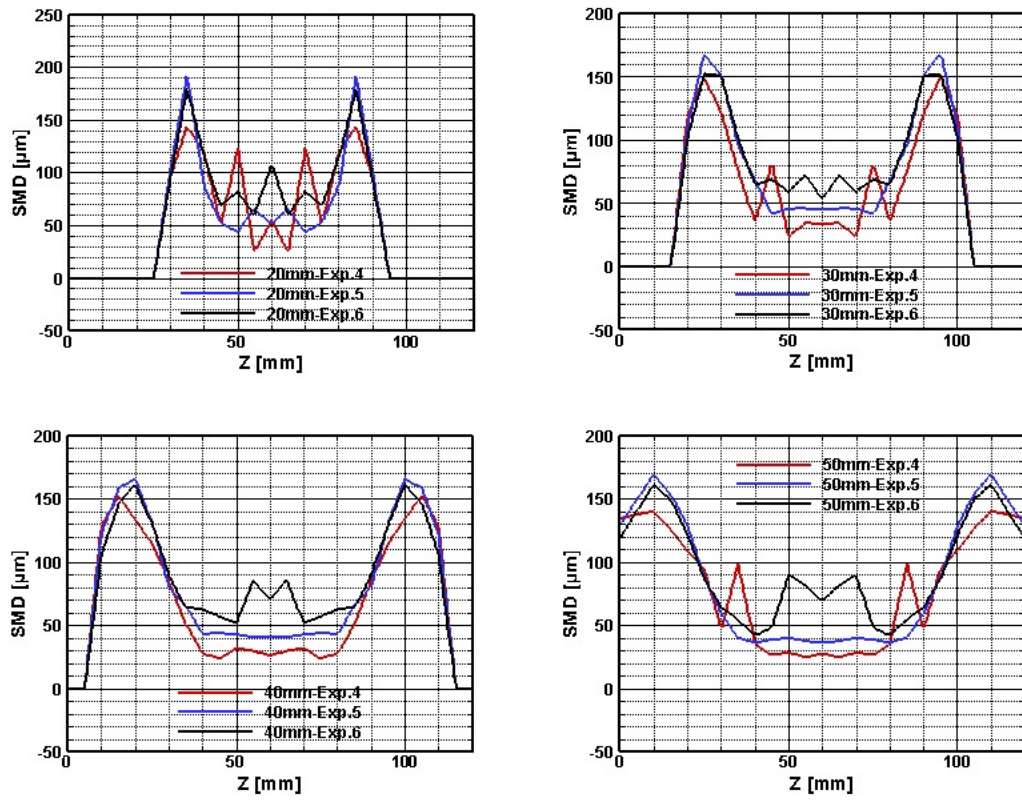


Figure A.3 SMD Values for Experiment 4,5 and 6

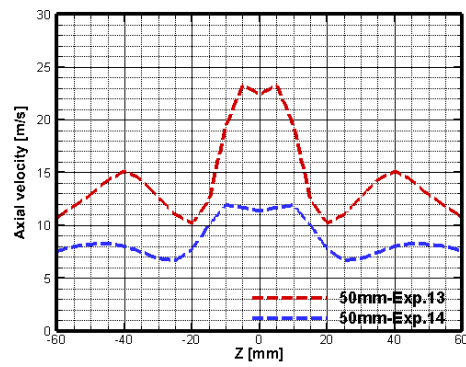
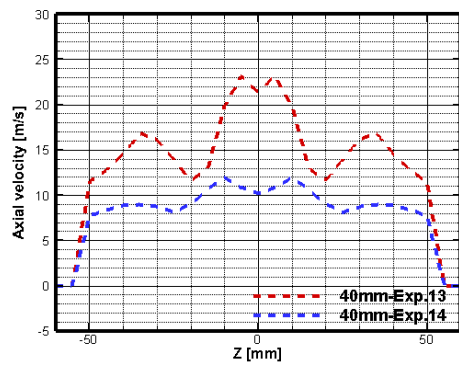
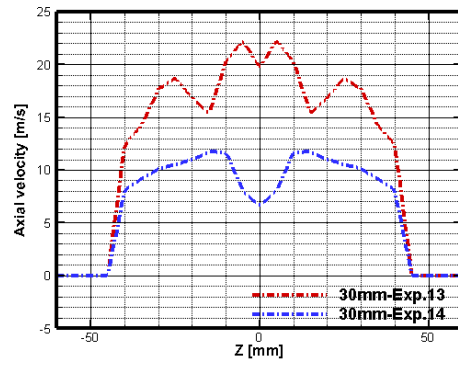
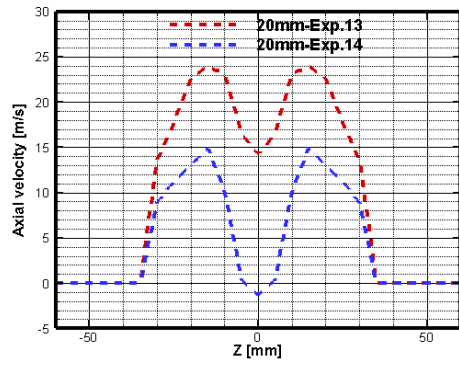


Figure A.4 Axial Velocities for Experiment 13 and 14

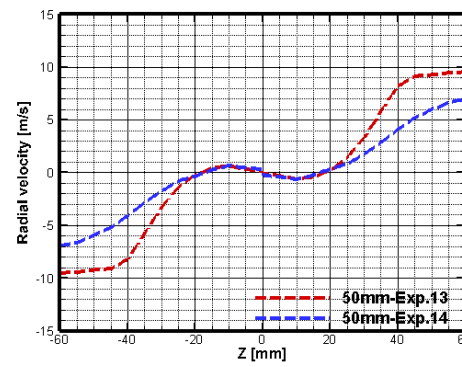
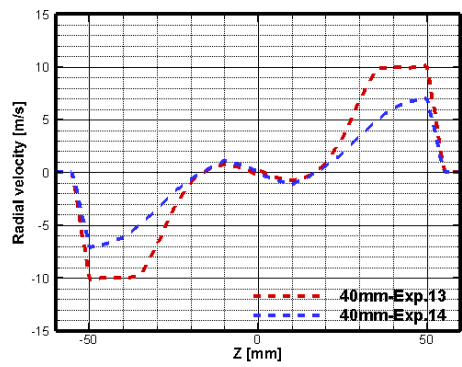
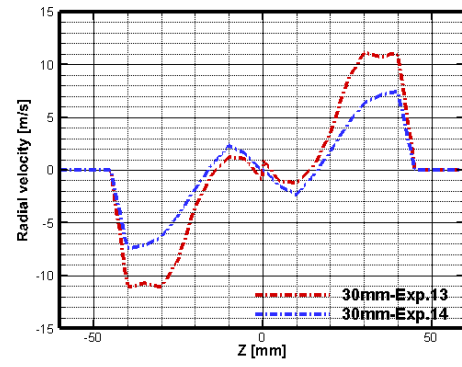
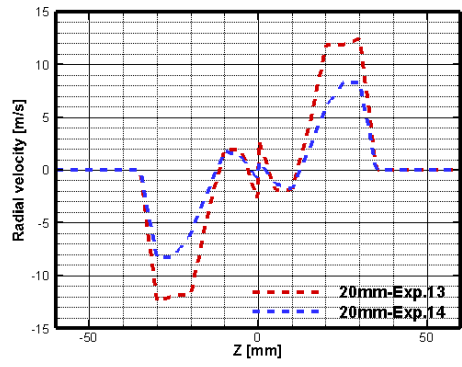


Figure A.5 Radial Velocities for Experiment 13 and 14

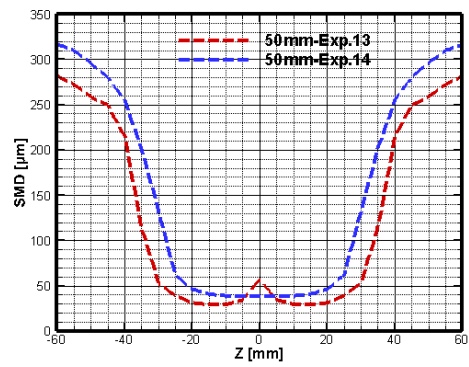
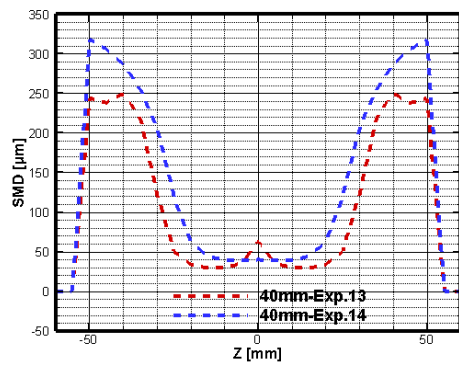
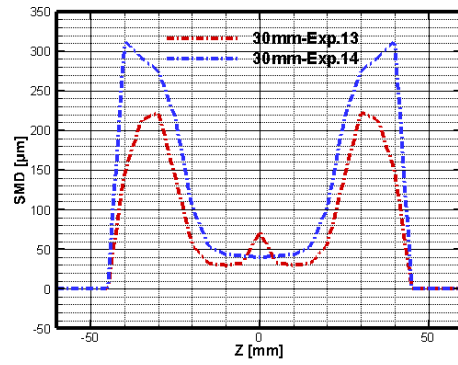
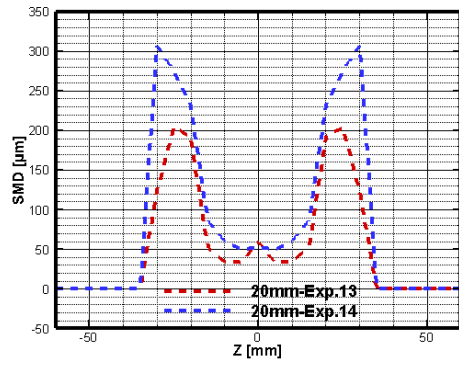


Figure A.6 SMD Values For Experiment 13 and 14

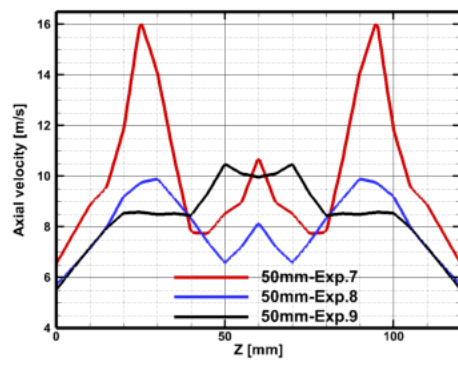
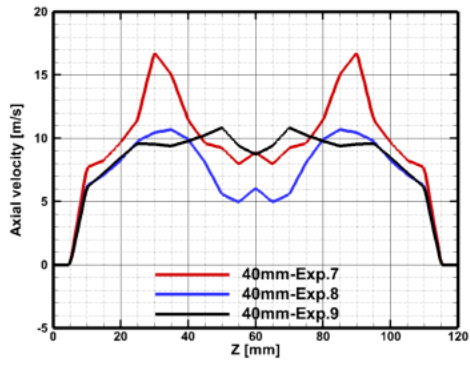
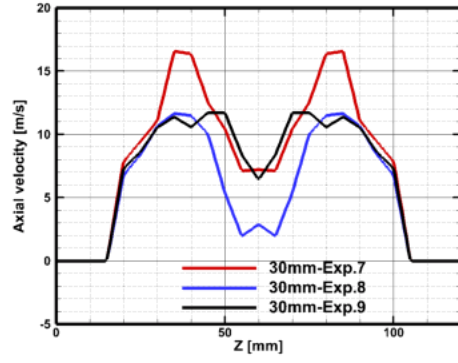
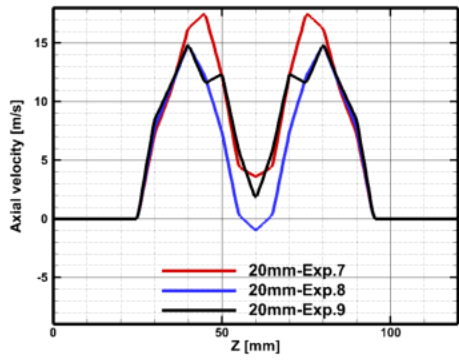


Figure A.7 Axial Velocities for Experiment 7,8 and 9

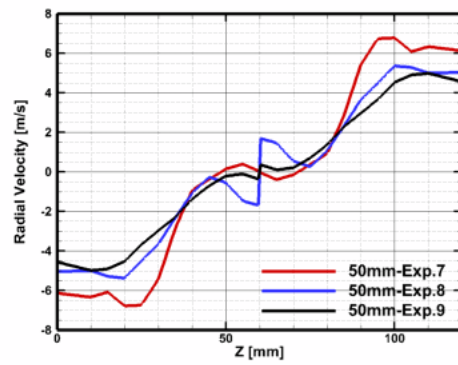
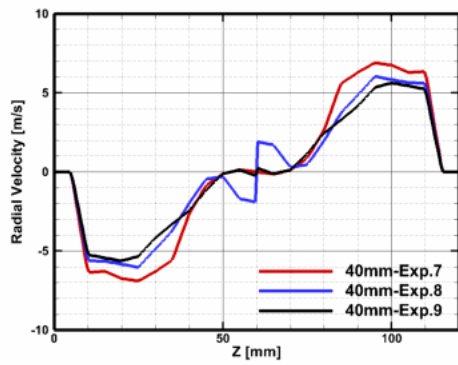
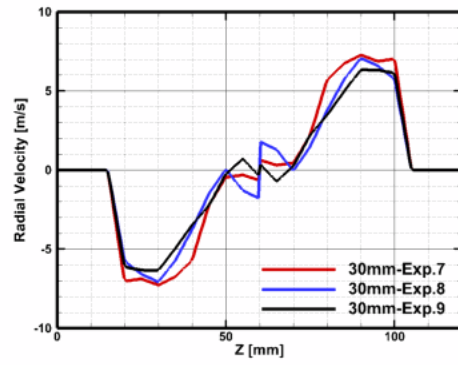
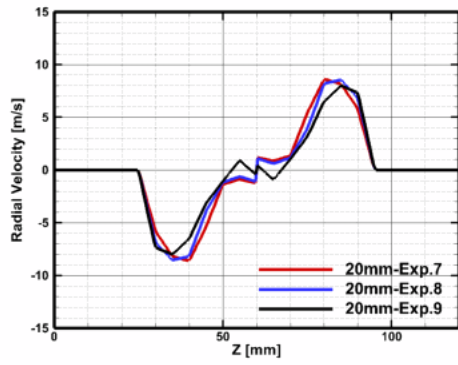


Figure A.8 Radial Velocites for Experiment 7,8 and 9

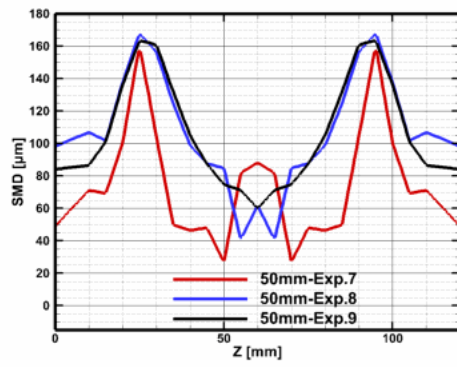
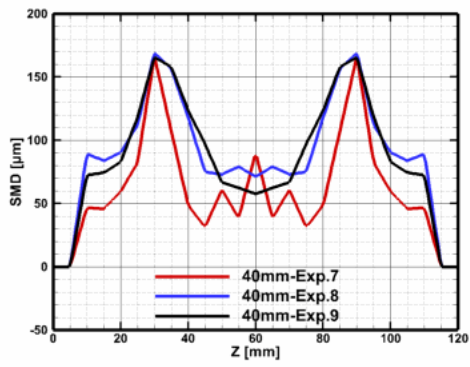
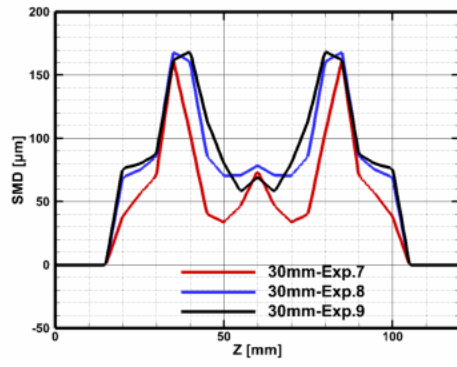
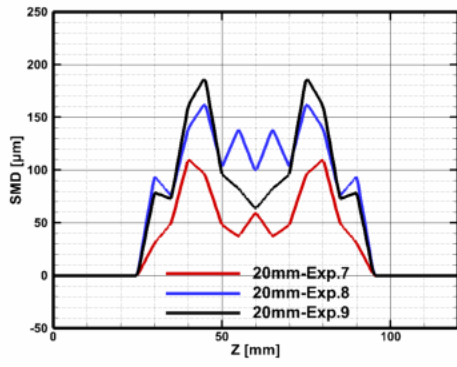


Figure A.9. SMD Values for Experiment 7,8 and 9

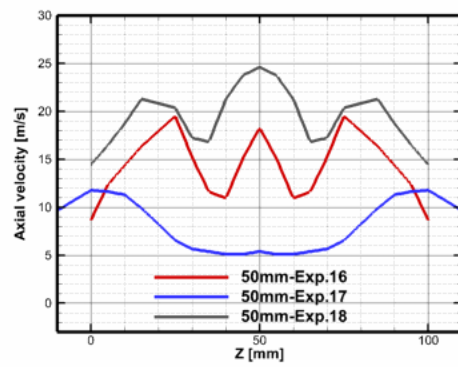
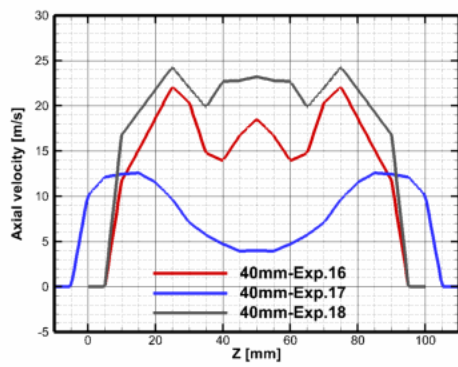
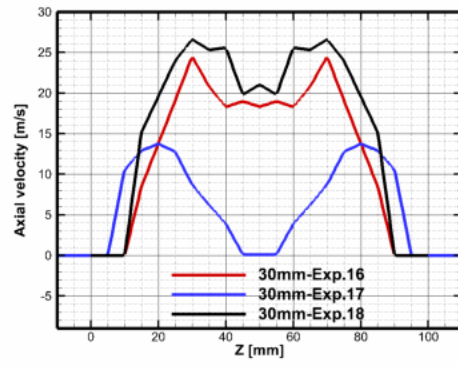
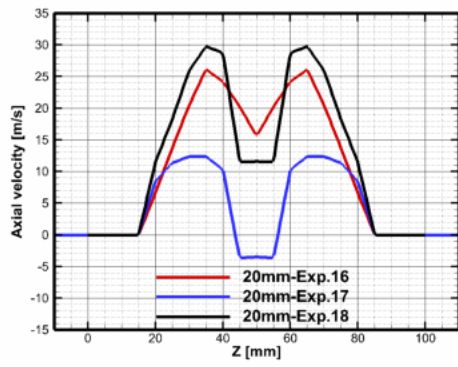


Figure A.10 Experiment 16,17 and 18

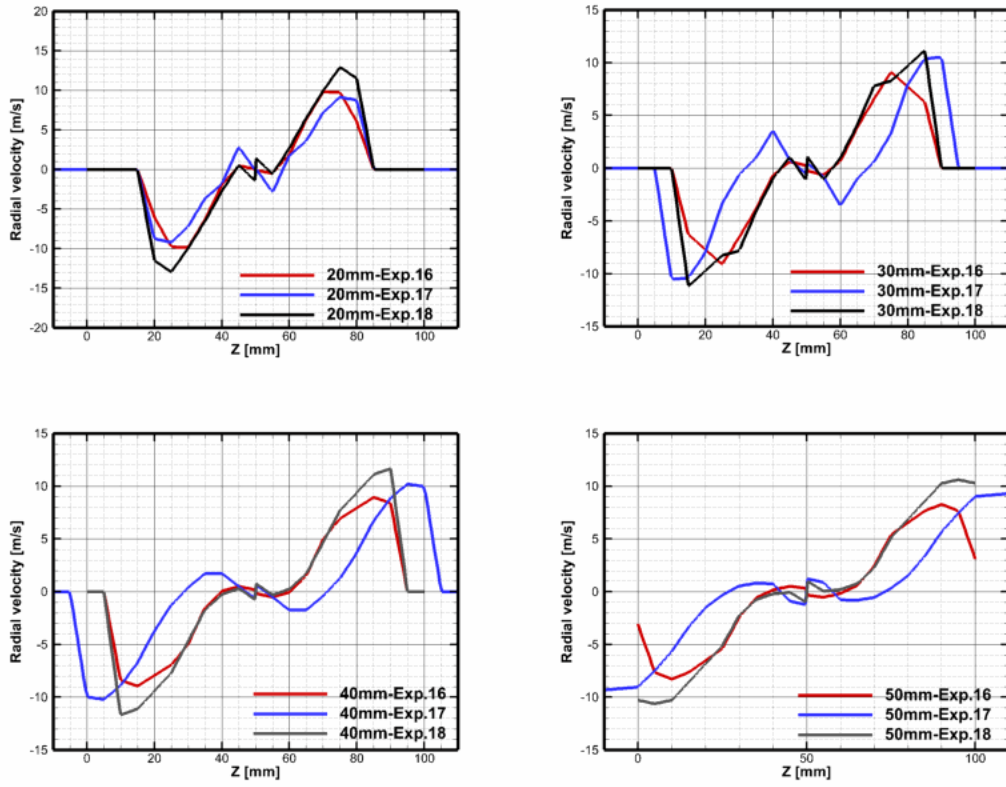


Figure A.11 Radial Velocities of Experiments 16,17 and 18

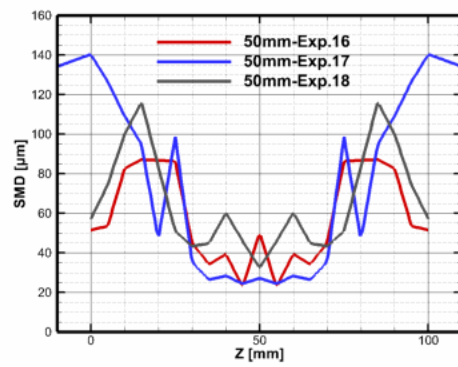
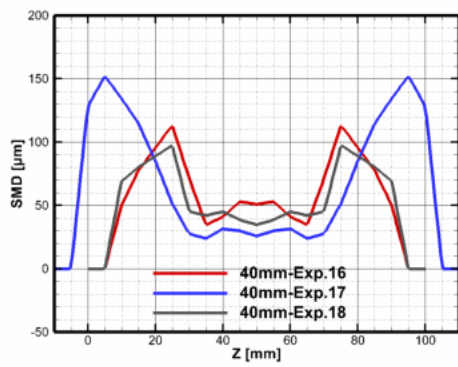
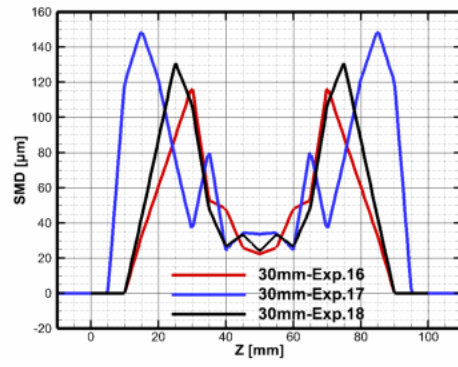
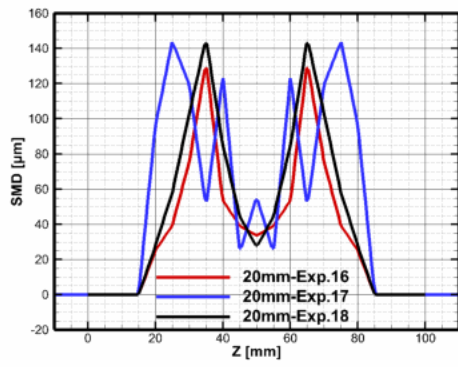


Figure A.12 SMD Values for Experiment 16,17 and 18